J. Fluid Mech. (1990), vol. 221, pp. 641–673
Printed in Great Britain

On near-wall turbulent flow modelling

By Y. G. LAI AND R. M. C. SO
Mechanical and Aerospace Engineering, Arizona State University, Tempe, AZ 85287, USA

(Received 23 January 1989 and in revised form 2 April 1990)

The characteristics of near-wall turbulence are examined and the result is used to assess the behaviour of the various terms in the Reynolds-stress transport equations. It is found that all components of the velocity-pressure-gradient correlation vanish at the wall. Conventional splitting of this second-order tensor into a pressure diffusion part and a pressure redistribution part and subsequent neglect of the pressure diffusion term in the modelled Reynolds-stress equations leads to finite near-wall values for two components of the redistribution tensor. This, therefore, suggests that, in near-wall turbulent flow modelling, the velocity-pressure-gradient correlation rather than pressure redistribution should be modelled. Based on this understanding, a methodology to derive an asymptotically correct model for the velocity-pressure-gradient correlation is proposed. A model that has the property of approaching the high-Reynolds-number model for pressure redistribution far away from the wall is derived. A similar analysis is carried out on the viscous dissipation term and asymptotically correct near-wall modifications are proposed. The near-wall closure based on the Reynolds-stress equations and a conventional low-Reynolds-number dissipation-rate equation is used to calculate fully-developed turbulent channel and pipe flows at different Reynolds numbers. A careful parametric study of the model constants introduced by the near-wall closure reveals that one constant in the dissipation-rate equation is Reynolds-number dependent, and a preliminary expression is proposed for this constant. With this modification, excellent agreement with near-wall turbulence statistics, measured and simulated, is obtained, especially the anisotropic behaviour of the normal stresses. On the other hand, it is found that the dissipation-rate equation has a significant effect on the calculated Reynolds-stress budgets. Possible improvements could be obtained by using available direct simulation data to help formulate a more realistic dissipation-rate equation. When such an equation is available, the present approach can again be used to derive a near-wall closure for the Reynolds-stress equations. The resultant closure could give improved predictions of the turbulence statistics and the Reynolds-stress budgets.

1. Introduction

The modelling of near-wall turbulent incompressible flow began with the work of van Driest (1956) who introduced a damping function for the mixing length to account for viscous effects near a wall. Since then, modifications of two-equation closures have been introduced by Jones & Launder (1972) and a host of other researchers. Fairly complete reviews of the development of two-equation near-wall turbulence closures have been provided by Patel, Rodi & Scheuerer (1985) and Launder (1986). In these reviews, attention was mainly concentrated on the k–ϵ type closures and little discussion was directed to other two-equation closures, such as that proposed by Hanjalic & Launder (1976). Most closures reviewed by Patel *et al.* (1985) do not solve the transport equation of the true dissipation rate, ϵ, of the

turbulent kinetic energy, k. Instead, they solved an equation that governs the dissipation rate, $\tilde{\epsilon}$, which is equal to the true dissipation rate minus its value at the wall. On the other hand, ϵ is retained in the k transport equation. As a result, most researchers found it necessary to modify both the k and the ϵ equations to account for viscous effects near a wall (e.g. Hoffmann 1975; Chien 1982), and to correctly reproduce the near-wall behaviour of k. This treatment is not quite correct because it leads to a near-wall behaviour of $\tilde{\epsilon} \sim y^2$ (Chien 1982), where y is the coordinate normal to the wall, while, in fact, $\tilde{\epsilon} \sim y$ near a wall (Shima 1988). Furthermore, even though the closures performed well for a wide range of turbulent flows (Patel *et al.* 1985), they have to be modified for diffuser flow calculations (Lai, So & Hwang 1989). Therefore, further modifications of these closures are necessary if an asymptotically correct near-wall, two-equation turbulence closure is to be available.

With the advent of supercomputers, many practical and complicated turbulent flows can now be calculated on a routine basis, even using more complex turbulence models such as Reynolds-stress closures. However, with some notable exceptions (e.g. Daly & Harlow 1970), nearly all studies in the past two decades or so invoked the wall-function approximations to describe the near-wall flow (Hanjalic & Launder 1972; Launder, Reece & Rodi 1975). The wall-function approximations are based on the assumptions of equilibrium turbulence and constant shear stress near a wall. These assumptions are less likely to be valid for complex turbulent wall shear flows and hence the need to develop near-wall Reynolds-stress closures. Efforts towards this direction have been made by Hanjalic & Launder (1976), by Prud'homme & Elghobashi (1983), by Kebede, Launder & Younis (1985), by So & Yoo (1986), by Launder & Tselepidakis (1988) and by Shima (1988), among others. With the exception of Hanjalic & Launder (1976) who solved the transport equations for the shear stress and k only, all other closures solved the Reynolds-stress transport equations suitably modified to account for viscous effects near a wall.

A common assumption made in all these closures is the splitting of the velocity-pressure-gradient correlation into a pressure diffusion part and a pressure redistribution part. The argument is then made that, since pressure diffusion is small across a wall shear layer (Laufer 1954), it can be neglected, even when the near-wall flow is modelled. Furthermore, it is also argued that, since viscosity does not appear explicitly in the Poisson equation for the fluctuating pressure, the high-Reynolds-number form of the redistribution model is also applicable for near-wall flow calculations. As a result, only the high-Reynolds-number isotropic form of the viscous dissipation rate model (e.g. Kolmogorov 1941) is modified to account for anisotropic behaviour near a wall. Even though the modifications (e.g. Hanjalic & Launder 1976; So & Yoo 1986) are not asymptotically correct as a wall is approached, the closures performed well for a wide variety of complex shear flows, including flows with wall transpiration (So & Yoo 1987), with sudden expansion (So *et al.* 1988; Yoo & So 1989) and with rotation (Yoo, So & Hwang 1990). On the other hand, Launder & Reynolds (1983) proposed an asymptotically correct near-wall dissipation model and it was applied by Kebede *et al.* (1985) to calculate periodic flow through a pipe. Reasonable agreement with measurements was achieved. Shima (1988) proposed a Reynolds-stress closure based on Lumley's (1980) rearrangement of the viscous dissipation and redistribution terms and a proposed modification for the wall correction of Launder *et al.*'s (1975) redistribution model. His results showed limited success for fully-developed pipe flow calculations.

All the above near-wall Reynolds-stress closures employed a dissipation-rate equation to close the set of governing equations. The dissipation-rate equation used

was either similar to the one employed in two-equation k–ϵ closures (Patel *et al.* 1985) or to the one proposed by Shima (1988). Since these dissipation-rate equations are derived in an ad hoc manner, their deficiencies could have a significant effect on the performance of the near-wall Reynolds-stress closures. Furthermore, some components of the redistribution model do not go to zero as the wall is approached, thus rendering the modelled Reynolds-stress equations incorrect near a wall. A consequence of this incorrect modelling is the inability to predict the anisotropic behaviour of the normal stresses near a wall (Hanjalic & Launder 1976; So & Yoo 1986). In view of these shortcomings, the near-wall Reynolds-stress closures are also not asymptotically correct as a wall is approached. Therefore, further modifications are necessary.

Based on the above discussion, it is clear that, in order to arrive at an asymptotically correct near-wall Reynolds-stress closure, improvements on the modelling of the Reynolds-stress equations as well as the dissipation-rate equation are required. Recognizing the difficulty of accomplishing this overall objective at this time, it is proposed to make a first attempt to formulate a general approach to derive an asymptotically correct near-wall closure for the Reynolds-stress equations using available high-Reynolds-number models for pressure redistribution and viscous dissipation and an existing dissipation-rate equation. When a more correct dissipation-rate equation and better high-Reynolds-number models based on stress invariant analyses are available, the proposed approach can again be used to derive an asymptotically correct near-wall Reynolds-stress closure. In order to illustrate the approach, a specific near-wall Reynolds-stress closure is proposed. It is based on the high-Reynolds-number model of Launder *et al.* (1975) for pressure redistribution and Kolmogorov's (1941) model for viscous dissipation far away from a wall and on Shima's (1988) low-Reynolds-number dissipation-rate equation. The validity of the approach and the proposed closure is verified by comparison with the simulation data of Kim, Moin & Moser (1987), the measurements of Laufer (1954) and Schildknecht, Miller & Meier (1979) and the model calculations of Hanjalic & Launder (1976), So & Yoo (1986) and Chien (1982). Finally, the ability of the closure to predict the simulated terms of the budgets of $\overline{u_i u_j}$ (Mansour, Kim & Moin 1988) is also examined.

2. Near-wall behaviour of the Reynolds-stress equations

The Reynolds-stress transport equations for an incompressible turbulent flow can be conveniently written in Cartesian tensor form as

$$\frac{\mathrm{D}\overline{u_i u_j}}{\mathrm{D}t} = \frac{\partial}{\partial x_k}(-\overline{u_i u_j u_k}) + \frac{\partial}{\partial x_k}\left(\nu\frac{\partial \overline{u_i u_j}}{\partial x_k}\right) - \left[\overline{u_i u_k}\frac{\partial U_j}{\partial x_k} + \overline{u_j u_k}\frac{\partial U_i}{\partial x_k}\right] - \frac{1}{\rho}\left[\overline{u_i\frac{\partial p}{\partial x_j}} + \overline{u_j\frac{\partial p}{\partial x_i}}\right] - 2\nu\overline{\frac{\partial u_i}{\partial x_k}\frac{\partial u_j}{\partial x_k}}, \quad (1)$$

or symbolically as

$$C_{ij} = D_{ij}^T + D_{ij}^\nu + P_{ij} + \Phi_{ij}^* - \epsilon_{ij}, \quad (2)$$

where x_i is the ith component of the coordinate, u_i and U_i are the ith components of the fluctuating and mean velocity, respectively, p is the fluctuating pressure, ρ and ν are fluid density and kinematic viscosity, respectively. With the exception of Φ_{ij}^*, the near-wall behaviour of every term in (2) can be analysed if the behaviour of u_i and U_i near a wall is known. Thus, (2) can be used to analyse the asymptotic behaviour of Φ_{ij}^* near a wall.

	C_{ij}	$-D^T_{ij}$	$-D^\nu_{ij}$	$-P_{ij}$	$+\epsilon_{ij}$
Φ^*_{11}	$O(y^3)$	$O(y^3)$	$-2\nu\overline{a_1^2}$ $-12\nu\overline{a_1 a_2}\,y$ $-O(y^2)$	$O(y^3)$	$2\nu\overline{a_1^2}+8\nu\overline{a_1 a_2}\,y+O(y^2)$
Φ^*_{33}	$O(y^3)$	$O(y^3)$	$-2\nu\overline{c_1^2}$ $-12\nu\overline{c_1 c_2}\,y$ $-O(y^2)$	$O(y^3)$	$2\nu\overline{c_1^2}+8\nu\overline{c_1 c_2}\,y+O(y^2)$
Φ^*_{13}	$O(y^3)$	$O(y^3)$	$-2\nu\overline{a_1 c_1}$ $-6\nu(\overline{a_1 c_2}+\overline{a_2 c_1})\,y$ $-O(y^2)$	$O(y^3)$	$2\nu\overline{a_1 c_1}+4\nu(\overline{a_1 c_2}+\overline{a_2 c_1})y+O(y^2)$
Φ^*_{12}	$O(y^4)$	$O(y^4)$	$-6\nu\overline{a_1 b_2}\,y$ $-O(y^2)$	$O(y^4)$	$4\nu\overline{a_1 b_2}\,y+O(y^2)$
Φ^*_{23}	$O(y^4)$	$O(y^4)$	$-6\nu\overline{b_2 c_1}\,y$ $-O(y^2)$	$O(y^4)$	$4\nu\overline{b_2 c_1}\,y+O(y^2)$
Φ^*_{22}	$O(y^5)$	$O(y^5)$	$-12\nu\overline{b_2^2}\,y^2$ $-O(y^3)$	$O(y^5)$	$8\nu\overline{b_2^2}\,y^2+O(y^3)$

TABLE 1. Near-wall behaviour of Φ^*_{ij}

The following expansions for u_i can be assumed in the near-wall region, or

$$\left.\begin{aligned} u &= a_1 y + a_2 y^2 + a_3 y^3 + \ldots, \\ v &= b_1 y + b_2 y^2 + b_3 y^3 + \ldots, \\ w &= c_1 y + c_2 y^2 + c_3 y^3 + \ldots, \end{aligned}\right\} \tag{3}$$

where $u_i = (u, v, w)$ and $x_i = (x, y, z)$ are substituted and y is taken to be normal to the wall, x is the stream direction and z is normal to the (x, y)-plane. The coefficients a_i, b_i, c_i are random functions of time and x and z, but not y. Since u_i has to satisfy the divergence condition because of incompressibility, it can be shown that $b_1 \equiv 0$. With these expansions, the linear behaviour of u'/u_τ (where $u' = (\overline{u^2})^{\frac{1}{2}}$, $u_\tau^2 = \tau_w/\rho$ and τ_w is the wall shear stress) near a wall as indicated by the measurements of Kreplin & Eckelmann (1979) can be recovered. For a two-dimensional flow, the above data also shows that $U \sim y$ near a wall, where $U_i = (U, V, 0)$, and continuity requires that $V \sim y^2$. The behaviour of Φ^*_{ij} can now be analysed and the result is tabulated in table 1 according to the rearranged form, $\Phi^*_{ij} = C_{ij} - D^T_{ij} - D^\nu_{ij} - P_{ij} + \epsilon_{ij}$.

The above analysis shows that C_{ij}, D^T_{ij} and P_{ij} go to zero at the wall like y^n, where $n \geqslant 3$. On the other hand, ϵ_{ij} and D^ν_{ij} are dominant near a wall and their difference has to be compensated by Φ^*_{ij}. If a model for Φ^*_{ij} is chosen such that Φ^*_{ij} is exactly zero at the wall but fails to balance the difference $(\epsilon_{ij} - D^\nu_{ij})$, at least to the lowest order, then the model cannot be expected to mimic the anisotropic behaviour of near-wall turbulence very well. Therefore, it is important to propose a near-wall Φ^*_{ij} model which can provide balance to the difference $(\epsilon_{ij} - D^\nu_{ij})$. Since D^T_{ij} is of order $y^n (n \geqslant 3)$ in the near-wall region, it can be approximated by high-Reynolds-number models. In the following, the models for D^T_{ij} and ϵ_{ij} are first discussed. Then the rationale for modelling Φ^*_{ij} is outlined and a proposal made for Φ^*_{ij}. Finally, an asymptotically correct dissipation-rate equation is presented to complete the closure of (2).

3. Near-wall Reynolds-stress closure

Numerous models have been proposed for D_{ij}^T. Among these, the four commonly-used models are due to Daly & Harlow (1970), Hanjalic & Launder (1972), Shir (1973) and Cormack, Leal & Steinfeld (1978). All four models expressed $\overline{u_i u_j u_k}$ in terms of $\overline{u_i u_j}$ and their gradients. Consequently, the near-wall behaviour of these models is consistent with that shown in table 1 for D_{ij}^T. At least, none of the D_{ij}^T models goe to zero like y^2 near a wall. In their study of third-order closures, Amano & Goel (1987) found that the model of Hanjalic & Launder (1972) gave the best overall results for the backward-facing step flow considered. Furthermore, in the near-wall region, the contribution of D_{ij}^T to the Reynolds-stress equations is small compared to that due to D_{ij}^{ν} (Laufer 1954; Hanjalic & Launder 1976; Mansour *et al.* 1988). In view of this, the model proposed by Hanjalic & Launder (1972) for D_{ij}^T is adopted here; namely,

$$D_{ij}^T = \frac{\partial}{\partial x_k}\left\{C_s \frac{k}{\epsilon}\left[\{\overline{u_i u_l}\}\frac{\partial \overline{u_j u_k}}{\partial x_l} + \{\overline{u_j u_l}\}\frac{\partial \overline{u_k u_i}}{\partial x_l} + \{\overline{u_k u_l}\}\frac{\partial \overline{u_i u_j}}{\partial x_l}\right]\right\}, \tag{4}$$

where C_s is a model constant.

The near-wall behaviour of ϵ_{ij} is given in table 1. If (3) is assumed for u_i, then, since $k = \frac{1}{2}\overline{u_i u_i}$ and $\epsilon = \nu(\overline{\partial u_i/\partial x_k})^2$, it can be shown that near a wall

$$k = \tfrac{1}{2}(\overline{a_1^2} + \overline{c_1^2})\, y^2 + (\overline{a_1 a_2} + \overline{c_1 c_2})\, y^3 + \tfrac{1}{2}A y^4 + O(y^5), \tag{5}$$

$$\epsilon = \nu(\overline{a_1^2} + \overline{c_1^2}) + 4\nu(\overline{a_1 a_2} + \overline{c_1 c_2})\, y + B\nu y^2 + O(y^3), \tag{6}$$

where

$$A = \overline{a_2^2} + 2\overline{a_1 a_3} + \overline{b_2^2} + \overline{c_2^2} + 2\overline{c_1 c_3},$$

$$B = \overline{\left(\frac{\partial a_1}{\partial x}\right)^2} + 4\overline{a_2^2} + 6\overline{a_1 a_3} + \overline{\left(\frac{\partial a_1}{\partial z}\right)^2} + 4\overline{b_2^2} + \overline{\left(\frac{\partial c_1}{\partial x}\right)^2} + 4\overline{c_2^2} + 6\overline{c_1 c_3} + \overline{\left(\frac{\partial c_1}{\partial z}\right)^2}.$$

According to Launder & Reynolds (1983), in the vicinity of a wall, the behaviour of $\epsilon_{ij}/\overline{u_i u_j}$ can be deduced from (3), (5) and (6) as

$$\frac{\epsilon_{11}}{\overline{u_1^2}} = \frac{\epsilon_{33}}{\overline{u_3^2}} = \frac{\epsilon_{13}}{\overline{u_1 u_3}} = \frac{\epsilon}{k}, \tag{7}$$

$$\frac{\epsilon_{12}}{\overline{u_1 u_2}} = \frac{\epsilon_{32}}{\overline{u_2 u_3}} = \frac{2\epsilon}{k}, \tag{8}$$

$$\frac{\epsilon_{22}}{\overline{u_2^2}} = \frac{4\epsilon}{k}. \tag{9}$$

Therefore, the near-wall behaviour of ϵ_{ij} as given in table 1 can be satisfied by (7)–(9). Introducing the unit vector $n_k = (0, 1, 0)$ to mark the normal direction to the wall, a model for ϵ_{ij} can be proposed along the suggestions of Hanjalic & Launder (1976), Launder & Reynolds (1983) and Launder & Tselepidakis (1988); namely,

$$\epsilon_{ij} = \tfrac{2}{3}\epsilon(1 - f_{\omega,1})\,\delta_{ij} + \frac{f_{w,1}(\epsilon/k)\,[\overline{u_i u_j} + \overline{u_i u_k}\, n_k n_j + \overline{u_j u_k}\, n_k n_i + n_i n_j \overline{u_k u_l}\, n_k n_l]}{1 + 3\overline{u_k u_l}\, n_l n_k / 2k}, \tag{10}$$

where $f_{w,1} = \exp[-(R_T/150)^2]$ with $R_T = k^2/\nu\epsilon$ essentially guarantees that ϵ_{ij} will asymptote to Kolmogorov's (1941) model far away from the wall. The model differs slightly from that of Launder & Tselepidakis (1988) because it is not necessary to

invoke the assumption that $\overline{u_2^2}$ is small compared to $\overline{u_1^2}$ (or $\overline{u_3^2}$) in the ϵ_{11} (or ϵ_{33}) term. Therefore, (10) gives, the correct behaviour near a wall since R_T goes to zero like y^4 and $f_{w,1}$ goes to 1 quickly as the wall is approached. Furthermore, (10) contracts properly to 2ϵ.

In high-Reynolds-number closure of (2), the term Φ_{ij}^* is divided into two parts; namely

$$\Phi_{ij}^* = \Phi_{ij}^p + \Phi_{ij}, \tag{11}$$

where

$$\Phi_{ij}^p = -\frac{1}{\rho}\left[\frac{\partial(\overline{pu_i})}{\partial x_j} + \frac{\partial(\overline{pu_j})}{\partial x_i}\right], \tag{12}$$

$$\Phi_{ij} = \overline{\frac{p}{\rho}\left[\frac{\partial u_i}{\partial x_j} + \frac{\partial u_j}{\partial x_i}\right]}. \tag{13}$$

Φ_{ij}^p is known as the pressure diffusion part and Φ_{ij} is interpreted as pressure redistribution. Since Φ_{ij}^p is small compared to D_{ij}^T for high-Reynolds-number flow (Laufer 1954), it is normally neglected in Reynolds-stress closures. As a result, Φ_{ij}^* with a non-zero trace is now replaced by Φ_{ij} with a zero trace. In order that the model proposed for Φ_{ij} is tensorially correct, it should also have a zero trace. Therefore, the Φ_{ij} model cannot replicate the behaviour of Φ_{ij}^* correctly near a wall. According to table 1, the various terms in (2) will be out of balance in the near-wall region and the closure will not be able to perform well because Φ_{23} and Φ_{12} are of order y^0 and Φ_{11}, Φ_{22}, Φ_{33} and Φ_{13} are of order y^1 owing to a non-vanishing p at the wall. On the other hand, most models for Φ_{ij} perform well far away from the wall (Mansour *et al.* 1988) and essentially validate the splitting of Φ_{ij}^* according to (11) and the neglect of Φ_{ij}^p for high-Reynolds-number flows (Launder *et al.* 1975). In view of this, it is suggested that Φ_{ij}^* be modelled in such a way that far away from the wall Φ_{ij}^* should approach Φ_{ij}. However, in the near-wall region, the model would balance the term $(\epsilon_{ij} - D_{ij}^\nu)$, at least to the lowest order shown in table 1 for each component. Several alternatives are available for the modelling of Φ_{ij}^* in the near-wall region. One, of course, is to model Φ_{ij}^p by a diffusion term in the near-wall flow. However, this approach requires the asymptotic behaviour of Φ_{ij}^p very near the wall to be known. Since this is not known *a priori*, this approach is not fruitful. Another approach is to model Φ_{ij}^* near a wall, because its near-wall behaviour is known from table 1. However, the proposed model should asymptote correctly to Φ_{ij} far away from a wall. Based on this argument, the following proposal is made for Φ_{ij}^*; namely,

$$\Phi_{ij}^* = \Phi_{ij} + \Phi_{ij,w} f_{w,1}, \tag{14}$$

where $f_{w,1}$ is introduced to guarantee the disappearance of $\Phi_{ij,w}$ far away from the wall. It should be pointed out that $\Phi_{ij,w} f_{w,1}$ is not proposed to model the term Φ_{ij}^p alone. Rather, it should be interpreted as the model for the pressure diffusion term Φ_{ij}^p plus the adjustment for the incorrect modelling of Φ_{ij} near a wall.

The proposal for $\Phi_{ij,w}$ depends to a large extent on the model for Φ_{ij}. Since Launder *et al.*'s model (1975) for Φ_{ij} accounts for both turbulence and mean-strain effects and is quite successful for a wide variety of complex flows, it is adopted for Φ_{ij} as a first attempt to derive a closure for the Reynolds-stress equations. The model for Φ_{ij}, therefore, is

$$\Phi_{ij} = -C_1 \frac{\epsilon}{k}(\overline{u_i u_j} - \tfrac{2}{3}\delta_{ij} k) - \alpha(P_{ij} - \tfrac{2}{3}\delta_{ij}\tilde{P}) - \beta(D_{ij} - \tfrac{2}{3}\tilde{P}\delta_{ij}) - \gamma k\left(\frac{\partial U_i}{\partial x_j} + \frac{\partial U_j}{\partial x_i}\right) \tag{15}$$

Component	C_1 term	α term	β term	γ term	Modelled Φ^*_{ij}
11	$-\frac{2}{3}\nu C_1(2\overline{a_1^2}-\overline{c_1^2})$ $-\frac{4}{3}\nu C_1(2\overline{a_1 a_2}-\overline{c_1 c_2})\,y+O(y^2)$	$O(y^3)$	$O(y^3)$	$O(y^3)$	$O(y^3)$
33	$-\frac{2}{3}\nu C_1(2\overline{c_1^2}-\overline{a_1^2})$ $-\frac{4}{3}\nu C_1(2\overline{c_1 c_2}-\overline{a_1 a_2})\,y+O(y^2)$	$O(y^3)$	$O(y^3)$	$O(y^3)$	$O(y^3)$
13	$-2\nu C_1\overline{a_1 c_1}-2\nu C_1(\overline{a_1 c_2}$ $+\overline{a_2 c_1})\,y+O(y^2)$	$O(y^3)$	$O(y^3)$	$O(y^3)$	$O(y^3)$
12	$-2\nu C_1\overline{a_1 b_2}\,y+O(y^2)$	$O(y^4)$	$O(y^4)$	$O(y^2)$	$-2\nu\overline{a_1 b_2}\,y$ $+O(y^2)$
23	$-2\nu C_1\overline{b_2 c_1}\,y+O(y^2)$	$O(y^4)$	$O(y^4)$	$O(y^2)$	$-2\nu\overline{b_2 c_1}\,y$ $+O(y^2)$
22	$\frac{2}{3}\nu C_1(\overline{a_1^2}+\overline{c_1^2})+\frac{4}{3}\nu C_1(\overline{a_1 a_2}$ $+\overline{c_1 c_2})\,y+O(y^2)$	$O(y^5)$	$O(y^5)$	$O(y^3)$	$-4\nu\overline{b_2^2}\,y^2$ $+O(y^3)$

TABLE 2. Near-wall behaviour of Φ_{ij} and the modelled Φ^*_{ij}

where
$$D_{ij}=\left[\overline{u_i u_k}\frac{\partial U_k}{\partial x_j}+\overline{u_j u_k}\frac{\partial U_k}{\partial x_i}\right],$$

$\tilde{P}=\frac{1}{2}P_{ii}$, $\alpha=\frac{1}{11}(8+C_2)$, $\beta=\frac{1}{11}(8C_2-2)$, $\gamma=\frac{1}{55}(30C_2-2)$ and C_1 and C_2 are model constants. With the model for Φ_{ij} specified, its behaviour near a wall can then be analysed using (3). The result is given in table 2.

The modelling of $\Phi_{ij,\mathrm{w}}$ should be such that it would compensate for the incorrect behaviour of the C_1 term while providing additional terms to balance $(\epsilon_{ij}-D^{\nu}_{ij})$. Furthermore, according to Shima (1988) and Launder *et al.* (1975), $\Phi_{ij,\mathrm{w}}$ should also provide additional terms to account for wall reflection effects in the not-too-near-wall region. Taking all these considerations and the model for ϵ_{ij} into account, a reasonable proposal would be

$$\Phi_{ij,\mathrm{w}}=C_1\frac{\epsilon}{k}(\overline{u_i u_j}-\tfrac{2}{3}\delta_{ij}k)-\frac{\epsilon}{k}(\overline{u_i u_k}\,n_k n_j+\overline{u_j u_k}\,n_k n_i)+\alpha^*(P_{ij}-\tfrac{2}{3}\delta_{ij}\tilde{P}), \tag{16}$$

where α^* is a model constant introduced by Shima. Based on (14), (15) and (16) for Φ^*_{ij} and (10) for ϵ_{ij}, the near-wall behaviour of the modelled Φ^*_{ij} term can now be evaluated and the result is listed in table 2 for comparison with the behaviour of the actual Φ^*_{ij} term. It can be seen that the modelled Φ^*_{ij} term is correct to y^3 for the Φ^*_{22} component, to y^2 for the Φ^*_{12} and Φ^*_{23} components and to y for all other components. The α^* term is not important for small y but is of the same order as the other two terms as y increases away from the wall.

It should be pointed out that even though the present model for Φ^*_{ij} behaves correctly near a wall, an attempt to deduce the shape of $\overline{pu_i}$ across the whole flow from the Φ^*_{ij} model may not be fruitful. This could be seen by considering fully-developed channel flow. For such a flow, $\Phi^*_{ij}=\Phi^{\mathrm{p}}_{ii}=\Phi_{ii,\mathrm{w}}f_{\mathrm{w},1}=-(2/\rho)(\mathrm{d}\overline{pv}/\mathrm{d}y)$. Since $\Phi_{ii,\mathrm{w}}f_{\mathrm{w},1}$ is only valid near a wall, strictly speaking, the shape of $\overline{pv}$ across the whole flow cannot be correctly deduced by integration to the channel centreline. In the near-wall region, the shape of $\overline{pv}$ is given by

$$\overline{pv}=\overline{pv}(0)-\int_0^{y_s}\tfrac{1}{2}\rho\Phi_{ii,\mathrm{w}}f_{\mathrm{w},1}\,\mathrm{d}y,$$

and is only valid up to y_s, which is the location where $\Phi_{ij}^* \simeq \Phi_{ij}$. If the integration is carried out to $y = \frac{1}{2}H$, where H is the channel width, it will give the unacceptable condition of $\overline{pv}$ being finite either at the wall or at the channel centreline.

It should be further pointed out that models (10), (14) and (16) do not necessarily represent the best models for ϵ_{ij} and Φ_{ij}^*. They represent the results of a first attempt to derive an asymptotically correct near-wall Reynolds-stress closure based on available high-Reynolds-number models for ϵ_{ij} and Φ_{ij}^*. If physically more correct models for these terms are available, such as the modelling attempt of Launder & Tselepidakis (1988) from stress invariant consideration, then the present approach can again be used to derive the required near-wall models for ϵ_{ij} and Φ_{ij}^*. Furthermore, if direct simulation data on p is available, they could be used to estimate the behaviour of Φ_{ij}^{p} near a wall and, perhaps, a way could be found to model the near-wall behaviour of Φ_{ij}^{p} directly. For the present, modelling Φ_{ij}^* near a wall seems to be a reasonable alternative.

4. The dissipation-rate equation

Since ϵ is introduced into this problem through models (4), (10), (15) and (16), a transport equation for ϵ is required to complete the closure of (2). Hanjalic & Launder (1976) proposed an equation for ϵ that was supposed to be valid for near-wall flows. The equation can be written as

$$\frac{\mathrm{D}\epsilon}{\mathrm{D}t} = \frac{\partial}{\partial x_k}\left(\nu\frac{\partial\epsilon}{\partial x_k}\right) + \frac{\partial}{\partial x_k}\left(C_\epsilon\frac{k}{\epsilon}\overline{u_k u_i}\frac{\partial\epsilon}{\partial x_i}\right) + \psi + C_{\epsilon 1}\frac{\epsilon}{k}\tilde{P} - C_{\epsilon 2}f_\epsilon\frac{\epsilon\tilde{\epsilon}}{k}, \tag{17}$$

where ψ is an additional production term related to the mean field, $\tilde{\epsilon} = \epsilon - 2\nu(\partial k^{\frac{1}{2}}/\partial y)^2$, $f_\epsilon = 1 - \frac{2}{9}\exp[-(\frac{1}{6}R_{\mathrm{T}})^2]$ and C_ϵ, $C_{\epsilon 1}$ and $C_{\epsilon 2}$ are model constants. The near-wall behaviour of this equation has been analysed by Shima (1988). He found that an additional term,

$$\xi = f_{\mathrm{w},2}\left[(\tfrac{7}{9}C_{\epsilon 2} - 2)\frac{\epsilon\bar{\epsilon}}{k} - \frac{1}{2}\frac{\bar{\epsilon}^2}{k}\right], \tag{18}$$

has to be introduced into (17) to fulfil the coincidence of $\partial\epsilon/\partial t$ and $\partial(\nu\partial^2 k/\partial x_j\partial x_j)/\partial t$ at the wall. This requires that $\partial\epsilon/\partial t = \partial(\nu\partial^2 k/\partial x_j\partial x_j)/\partial t = -2\nu^2 B + 12\nu^2 A$. The function $f_{\mathrm{w},2} = \exp[-(R_{\mathrm{T}}/64)^2]$ is specified to guarantee that ξ goes to zero outside the near-wall region and the high-Reynolds-number form of the equation is recovered. In (18), $\bar{\epsilon}$ is defined as $(\epsilon - \nu\partial^2 k/\partial x_j\partial x_j)$. Shima also argued that since ψ essentially enhances ϵ generation in the immediate vicinity of a wall, its complex form can be avoided by replacing the term $(\psi + C_{\epsilon 1}\epsilon\tilde{P}/k)$ by $C_{\epsilon 1}(1 + \sigma f_{\mathrm{w},2})\epsilon\tilde{P}/k$, where $\sigma = 1$ has been suggested by Shima (1988). However, in the present study σ is found to be Reynolds-number dependent and its value will be discussed later.

The form of $\bar{\epsilon} = \epsilon - \nu\partial^2 k/\partial x_j\partial x_j$ proposed by Shima is not convenient numerically, because it involves the second derivatives of k in a region where k changes rapidly. A more convenient and numerically stable form for $\bar{\epsilon}$ is found to be

$$\epsilon^* = \epsilon - \frac{2\nu k}{y^2}. \tag{19}$$

If $\bar{\epsilon}$ in $\bar{\epsilon}^2/2k$ is replaced by (19) and $\bar{\epsilon}$ in $\epsilon\bar{\epsilon}/k$ is replaced by $\tilde{\epsilon}$, then the resultant form satisfies the coincidence condition and the near-wall behaviour examined by Shima. Consequently, the wall boundary condition for ϵ is $\epsilon = 2\nu(\partial k^{\frac{1}{2}}/\partial y)^2$ as $y \to 0$, rather

than the condition $\epsilon = \nu \partial^2 k/\partial x_j \partial x_j$. Later calculations show that this modification leads to rapid convergence of the governing equations for fully-developed channel and pipe flows and little or no oscillations of the numerical results.

5. An asymptotically correct k–ϵ closure

Contraction of (1) with the substitution of models (4), (10), (15) and (16) gives

$$2\frac{\mathrm{D}k}{\mathrm{D}t} = 2\frac{\partial}{\partial x_j}\left(\nu\frac{\partial k}{\partial x_j}\right) + 2\frac{\partial}{\partial x_j}\left(\frac{\nu_t}{\sigma_k}\frac{\partial k}{\partial x_j}\right) + 2\tilde{P} - \frac{\epsilon}{k} f_{w,1}(2\overline{u_i u_k} n_k n_i) - 2\epsilon, \tag{20}$$

where σ_k is a model constant and $\nu_t = C_\mu f_\mu k^2/\epsilon$ and $f_\mu = 1 - \exp(-C_3 y u_\tau/\nu)$ have been introduced to simplify (20). In the original equation for k, the diffusion coefficients are not isotropic. However, in anticipation of the gradient transport assumption, an isotropic ν_t is postulated. Therefore, it is necessary to introduce the function f_μ with model constant C_3 to account for reduced diffusion of k near a wall. This approximation is consistent with other proposals (Reynolds 1976; Lam & Bremhorst 1981; Chien 1982). The asymptotically correct k transport equation can be solved together with the modified near-wall form of (17) to give k and ϵ. The gradient transport assumption is made to complete the closure, and this gives the following equations for the asymptotically correct k–ϵ closure of turbulence:

$$\frac{\mathrm{D}k}{\mathrm{D}t} = \frac{\partial}{\partial x_j}\left(\nu\frac{\partial k}{\partial x_j}\right) + \frac{\partial}{\partial x_j}\left(\frac{\nu_t}{\sigma_k}\frac{\partial k}{\partial x_j}\right) + \tilde{P} - \epsilon - f_{w,1}\frac{\epsilon}{k}\overline{v^2}, \tag{21}$$

$$\frac{\mathrm{D}\epsilon}{\mathrm{D}t} = \frac{\partial}{\partial x_j}\left(\nu\frac{\partial \epsilon}{\partial x_j}\right) + \frac{\partial}{\partial x_j}\left(\frac{\nu_t}{\sigma_\epsilon}\frac{\partial \epsilon}{\partial x_j}\right) + C_{\epsilon 1}(1 + \sigma f_{w,2})\frac{\epsilon}{k}\tilde{P} - C_{\epsilon 2} f_\epsilon \frac{\epsilon\tilde{\epsilon}}{k} + \xi, \tag{22}$$

$$-\overline{u_i u_j} = \nu_t\left(\frac{\partial U_i}{\partial x_j} + \frac{\partial U_j}{\partial x_i}\right) - \tfrac{2}{3}\delta_{ij} k. \tag{23}$$

In view of the fact that $-\overline{u_i u_j}$ is given by (23), the turbulent diffusion term $\partial(C_\epsilon(k/\epsilon)\overline{u_k u_l}(\partial\epsilon/\partial x_l))/\partial x_k$ in (17) is again approximated by $\partial((\nu_t/\sigma_\epsilon)(\partial\epsilon/\partial x_k))/\partial x_k$, where the constant C_ϵ is now replaced by σ_ϵ.

This set of equations is different from those examined by Patel *et al.* (1985). Here, the true dissipation rate ϵ is solved with $\epsilon = 2\nu(\partial k^{\frac{1}{2}}/\partial y)^2$ specified at the wall. Furthermore, the correction to the k-equation is given by the term $f_{w,1}(\epsilon/k)(\overline{v^2})$, which represents the anisotropic behaviour of the modelled Φ_{ij}^* term, rather than by terms like $2\nu k/y^2$, $2\nu(\partial k^{\frac{1}{2}}/\partial y)^2$, etc., which do not represent the anisotropy of the velocity–pressure-gradient correlation. Near a wall $f_{w,1}(\epsilon/k)(\overline{v^2})$ is much smaller than ϵ and the viscous term in (21), because $v^2 \sim y^4$, and is practically zero away from the wall. Therefore, it can be neglected. Consequently, with the exception of the term $\partial(\nu(\partial k/\partial x_j))/\partial x_j$, (21) reduces to the high-Reynolds-number form. The reason the other researcher (e.g. Hoffmann 1975; Chien 1982) have to propose a modification to the k-equation for near-wall turbulence is because they are solving for $\tilde{\epsilon}$ rather than ϵ. On the other hand, the ϵ-equation has to be modified for near-wall flow modelling. As a result, the near-wall $k-\epsilon$ closures proposed by Reynolds (1976) and Lam & Bremhorst (1981), where they solved for ϵ but with no additional near-wall terms added to either the k- or the ϵ-equation, are also asymptotically incorrect near a wall.

6. Fully-developed pipe flow equations

A cylindrical coordinate system (x, r, θ) is chosen so that the fully-developed mean and fluctuating velocities in a pipe of radius R are given by $(U, 0, 0)$ and (u, v, w), respectively. The governing equations for this fully-developed pipe flow, written in terms of the proposed near-wall Reynolds-stress closure, are:

$$\nu\frac{\mathrm{d}U}{\mathrm{d}r}-\overline{uv}+\frac{ru_\tau^2}{R}=0, \tag{24}$$

$$\frac{1}{r}\frac{\mathrm{d}}{\mathrm{d}r}\left[r\left(\nu+C_\mathrm{s}\frac{k}{\epsilon}\overline{v^2}\right)\frac{\mathrm{d}\overline{u^2}}{\mathrm{d}r}\right]+\frac{1}{r}\frac{\mathrm{d}}{\mathrm{d}r}\left[rC_\mathrm{s}\frac{k}{\epsilon}2\overline{uv}\frac{\mathrm{d}\overline{uv}}{\mathrm{d}r}\right]-2(1-\tfrac{2}{3}\alpha+\tfrac{1}{3}\beta+\tfrac{2}{3}\alpha^* f_{\mathrm{w},1})\,\overline{uv}\frac{\mathrm{d}U}{\mathrm{d}r}$$
$$-C_1(1-f_{\mathrm{w},1})\frac{\epsilon}{k}(\overline{u^2}-\tfrac{2}{3}k)-\tfrac{2}{3}\epsilon(1-f_{\mathrm{w},1})-f_{\mathrm{w},1}\frac{\epsilon}{k}\overline{u^2}\Big/\left(1+\frac{3\overline{v^2}}{2k}\right)=0, \tag{25}$$

$$\frac{1}{r}\frac{\mathrm{d}}{\mathrm{d}r}\left[r\left(\nu+3C_\mathrm{s}\frac{k}{\epsilon}\overline{v^2}\right)\frac{\mathrm{d}\overline{v^2}}{\mathrm{d}r}\right]-\frac{2}{r}C_\mathrm{s}\frac{k}{\epsilon}\overline{v^2}\frac{\mathrm{d}\overline{w^2}}{\mathrm{d}r}-\frac{4}{r^2}C_\mathrm{s}\frac{k}{\epsilon}\overline{w^2}(\overline{v^2}-\overline{w^2})+\frac{2\nu}{r^2}(\overline{w^2}-\overline{v^2})$$
$$-\tfrac{2}{3}(\alpha-2\beta-\alpha^* f_{\mathrm{w},1})\,\overline{uv}\frac{\mathrm{d}U}{\mathrm{d}r}-C_1(1-f_{\mathrm{w},1})\frac{\epsilon}{k}(\overline{v^2}-\tfrac{2}{3}k)-\tfrac{2}{3}\epsilon(1-f_{\mathrm{w},1})$$
$$-2f_{\mathrm{w},1}\frac{\epsilon}{k}\overline{v^2}-4f_{\mathrm{w},1}\frac{\epsilon}{k}\overline{v^2}\Big/\left(1+\frac{3\overline{v^2}}{2k}\right)=0, \tag{26}$$

$$\frac{1}{r}\frac{\mathrm{d}}{\mathrm{d}r}\left[r\left(\nu+C_\mathrm{s}\frac{k}{\epsilon}\overline{v^2}\right)\frac{\mathrm{d}\overline{w^2}}{\mathrm{d}r}\right]+\frac{2}{r}\frac{\mathrm{d}}{\mathrm{d}r}\left[C_\mathrm{s}\frac{k}{\epsilon}\overline{w^2}(\overline{v^2}-\overline{w^2})\right]+\frac{4}{r^2}C_\mathrm{s}\frac{k}{\epsilon}\overline{w^2}(\overline{v^2}-\overline{w^2})+\frac{2}{r}C_\mathrm{s}\frac{k}{\epsilon}\overline{v^2}\frac{\mathrm{d}\overline{w^2}}{\mathrm{d}r}$$
$$+\frac{2\nu}{r^2}(\overline{v^2}-\overline{w^2})-\tfrac{2}{3}(\alpha+\beta-\alpha^* f_{\mathrm{w},1})\,\overline{uv}\frac{\mathrm{d}U}{\mathrm{d}r}-C_1(1-f_{\mathrm{w},1})\frac{\epsilon}{k}(\overline{w^2}-\tfrac{2}{3}k)$$
$$-\tfrac{2}{3}\epsilon(1-f_{\mathrm{w},1})-f_{\mathrm{w},1}\frac{\epsilon}{k}w^2\Big/\left(1+\frac{3\overline{v^2}}{2k}\right)=0, \tag{27}$$

$$\frac{1}{r}\frac{\mathrm{d}}{\mathrm{d}r}\left[r\left(\nu+2C_\mathrm{s}\frac{k}{\epsilon}\overline{v^2}\right)\frac{\mathrm{d}\overline{uv}}{\mathrm{d}r}\right]+\frac{1}{r}\frac{\mathrm{d}}{\mathrm{d}r}\left[rC_\mathrm{s}\frac{k}{\epsilon}\overline{uv}\frac{\mathrm{d}\overline{v^2}}{\mathrm{d}r}\right]-\frac{1}{r}C_\mathrm{s}\frac{k}{\epsilon}\overline{uv}\left(\frac{\mathrm{d}\overline{w^2}}{\mathrm{d}r}+\frac{2\overline{w^2}}{r}\right)-\frac{\nu}{r^2}\overline{uv}$$
$$-[(1-\alpha+\alpha^* f_{\mathrm{w},1})\,\overline{v^2}-\beta\overline{u^2}+\gamma k]\frac{\mathrm{d}U}{\mathrm{d}r}-C_1(1-f_{\mathrm{w},1})\frac{\epsilon}{k}\overline{uv}$$
$$-f_{\mathrm{w},1}\frac{\epsilon}{k}\overline{uv}-2f_{\mathrm{w},1}\frac{\epsilon}{k}\overline{uv}\Big/\left(1+\frac{3\overline{v^2}}{2k}\right)=0, \tag{28}$$

$$\frac{1}{r}\frac{\mathrm{d}}{\mathrm{d}r}\left[r\left(\nu+C_\epsilon\frac{k}{\epsilon}\overline{v^2}\right)\frac{\mathrm{d}\epsilon}{\mathrm{d}r}\right]-C_{\epsilon 1}(1+\sigma f_{\mathrm{w},2})\frac{\epsilon}{k}\overline{uv}\frac{\mathrm{d}U}{\mathrm{d}r}$$
$$-C_{\epsilon 2}f_\epsilon\frac{\epsilon\tilde{\epsilon}}{k}+f_{\mathrm{w},2}\left[(\tfrac{7}{9}C_{\epsilon 2}-2)\frac{\epsilon\tilde{\epsilon}}{k}-\frac{1}{2}\frac{\epsilon^{*2}}{k}\right]=0. \tag{29}$$

The model constants are the same as those specified by Hanjalic & Launder (1972, 1976), by Launder *et al.* (1975) and by Shima (1988). For completeness, they are given here as: $C_1 = 1.5$, $C_2 = 0.4$, $C_{\epsilon 1} = 1.35$, $C_{\epsilon 2} = 1.8$, $C_\mathrm{s} = 0.11$, $C_\epsilon = 0.15$ and $\alpha^* = 0.45$. Hanjalic & Launder (1976) and subsequently So & Yoo (1986) found it necessary to multiply the stress production term of (28) by a wall damping function

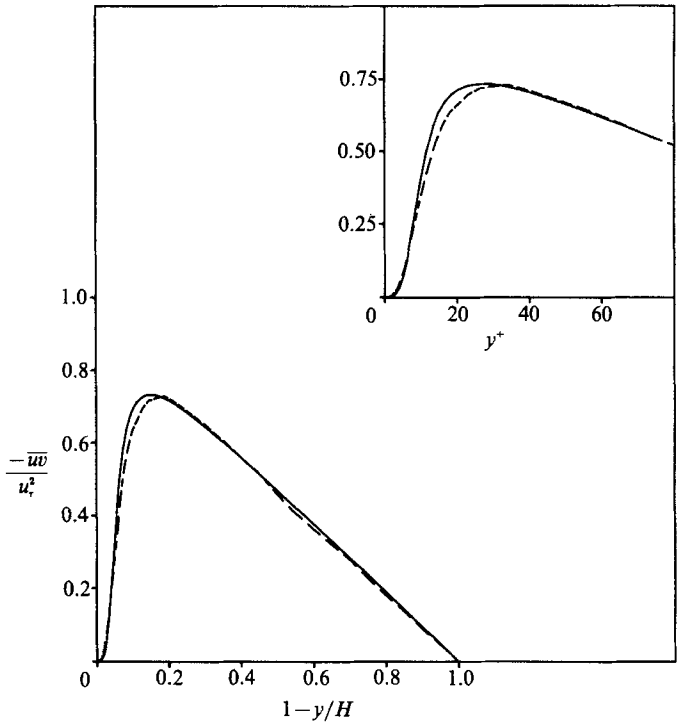

FIGURE 1. Comparison of modelled and simulation results for shear stress. ---, Kim *et al.* 1987; ——, present model.

to bring into balance near a wall the shear production with the other terms in (28). This arbitrary damping is unacceptable because the production term is exact and should not be modified. Hence, no such modification is used for the present near-wall model. The necessity of the damping function is just another indication that the near-wall model is not quite asymptotically correct.

Since the flow is axisymmetric, only boundary conditions at the wall and at the symmetry line are required. These can be specified as:

$$U = \overline{u^2} = \overline{v^2} = \overline{w^2} = \overline{uv} = 0, \quad \epsilon = 2\nu\left(\frac{\partial k^{\frac{1}{2}}}{\partial y}\right)^2 \quad \text{at } r = R, \tag{30}$$

$$\frac{\mathrm{d}\epsilon}{\mathrm{d}r} = \frac{d\overline{u^2}}{\mathrm{d}r} = \frac{d\overline{v^2}}{\mathrm{d}r} = \frac{d\overline{w^2}}{\mathrm{d}r} = 0, \quad \overline{uv} = 0 \quad \text{at } r = 0. \tag{31}$$

Here, $y = R - r$ is taken as positive away from the wall.

A similar set of equations can also be written down for the k–ϵ closure. The model constants are again taken to be the widely-accepted values: $\sigma_k = 1.0$, $\sigma_\epsilon = 1.3$, $C_3 = 0.0115$ and $C_\mu = 0.09$. Therefore, in both the Reynolds-stress and k–ϵ closures, all conventionally accepted constants for the high-Reynolds-number models are adopted. Similar sets of Reynold-stress and k–ϵ closure equations for channel flows can also be written down. Since they can be straight-forwardly obtained using Cartesian tensors, the channel flow equations are not reported here.

The governing equations are ordinary differential equations, therefore, they can be solved by any iteration scheme for split boundary-value problems (Na 1979). Here, the Newton iteration scheme used by So & Yoo (1986) is adopted. The dependent

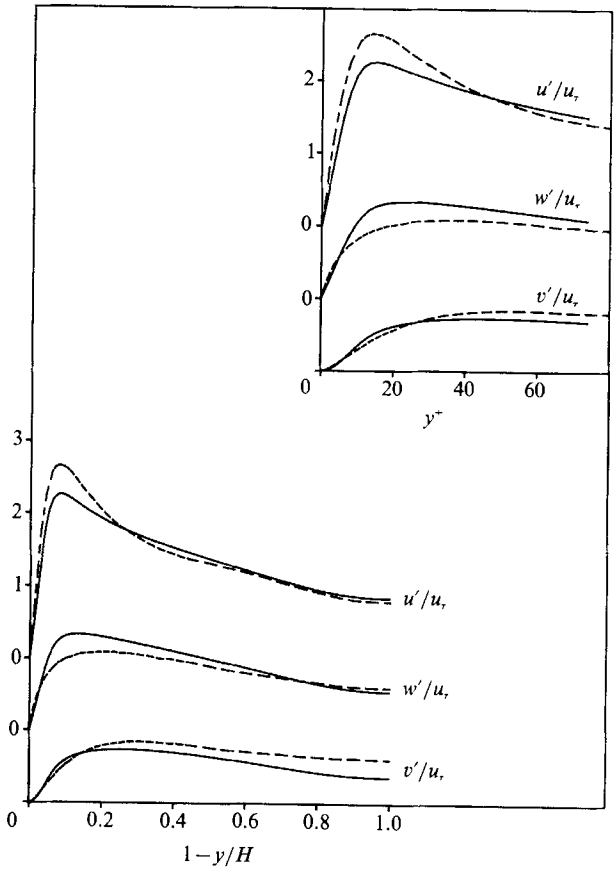

FIGURE 2. Comparison of modelled and simulation results for the normal stresses. ---, Kim *et al.* 1987; ——, present model.

variables are normalized by u_τ and u_τ^3/R while the r coordinate is normalized to become $y^+ = u_\tau(R-r)/\nu$. Integration from the pipe wall to the symmetry line is now carried out from $y^+ = 0$ to $y^+ = Re = u_\tau R/\nu$. Since $Re = (u_\tau/2U_0)Re_D$, where Re_D is defined as $2RU_0/\nu$ and U_0 is the mean bulk velocity, it serves as the only input parameter to the solution of (24)–(29) subject to boundary conditions (30) and (31).

The non-uniform grid proposed by So & Yoo (1986) is used for the present calculations. A total of 51 grid points are specified for the range $0 \leqslant y^+ \leqslant Re$, with 5 points specified between $y^+ = 0$ and 5 and 15 points located in the region $5 \leqslant y^+ \leqslant 65$. With this grid spacing, convergent solution satisfying an accuracy criterion of $\leqslant 10^{-5}$ for the residuals is possible after about one thousand iterations.

7. Comparison of the turbulence statistics

Two model constants, σ and α^*, are introduced in the near-wall Reynolds-stress closure. The other constants are associated with the high-Reynolds-number models adopted for the present proposal. Since these latter constants are well tested by other researchers, it seems prudent not to attempt to vary their values to fit measurements or direct simulation data. After all, the present proposed near-wall closure should asymptotically approach the high-Reynolds-number closure of Launder *et al.* (1975) far away from a wall. Although $\sigma = 1.0$ and $\alpha^* = 0.45$ are the reported choice of

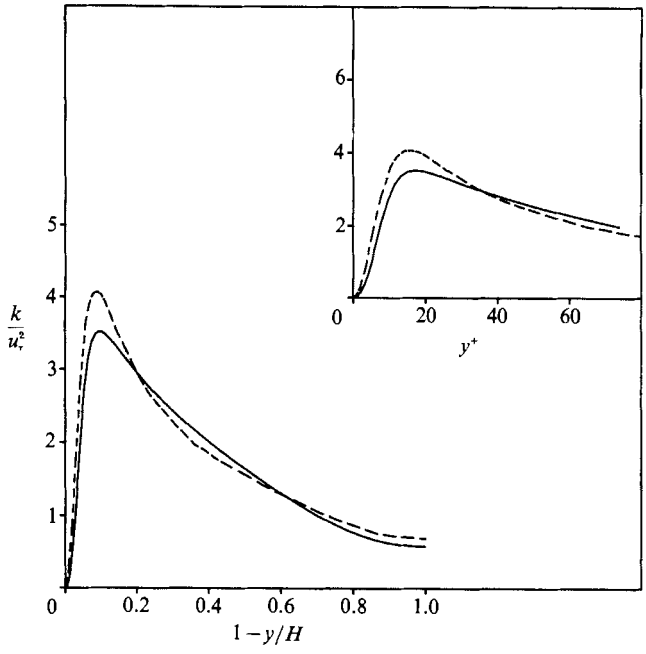

FIGURE 3. Comparison of modelled and simulation results for k.
---, Kim *et al.* 1987; ——, present model.

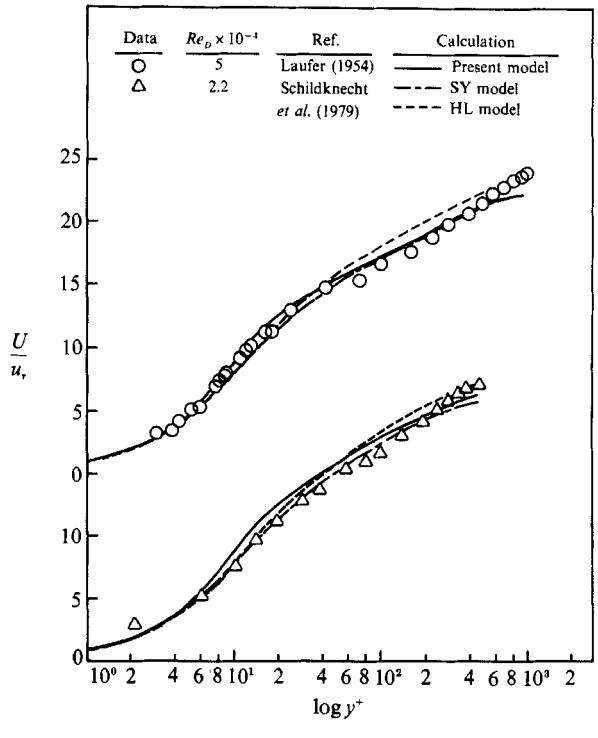

FIGURE 4. Comparison of Reynolds-stress closure calculations of U with data.

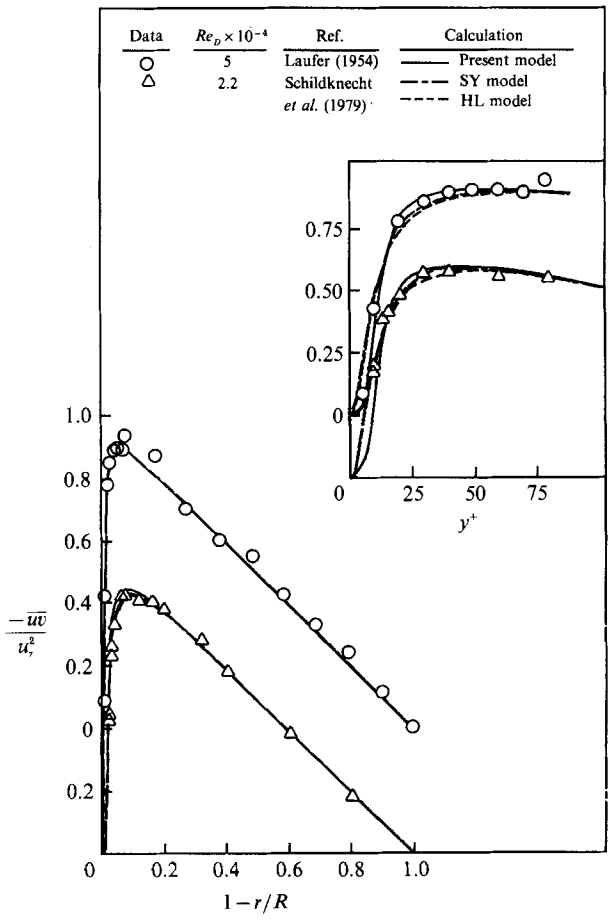

FIGURE 5. Comparison of Reynolds-stress closure calculations of $\overline{uv}$ with data.

Shima (1988), recent work by Mansour, Kim & Moin (1989) suggested that these constants might be Reynolds-number dependent. Initial calibrations of these constants with channel and pipe flow measurements at $Re_D > 20000$ reveal that $\sigma = 1.0$ and $\alpha^* = 0.45$ are indeed appropriate values for the closure. However, in the light of the low-Reynolds-number simulation data of Kim *et al.* (1987), the k–ϵ modelling analyses of Mansour *et al.* (1989) and the suggestion of a reviewer, a thorough parametric study of these two constants was carried out using both channel and pipe flow measurements and direct simulation data. Thus, the Re_D range covered varies from 6600 for Kim *et al.*'s (1987) data to 50000 for Laufer's (1954) measurements. The result shows that the calculated turbulence statistics are not much affected by varying α^* and that $\alpha^* = 0.45$ seems to give the overall best correlation with simulation data and measurements. On the other hand, just as Mansour *et al.* (1989) pointed out, σ is found to be Reynolds-number dependent. Based on this parametric study, a preliminary expression is proposed for σ, such that

$$\sigma = 1.0 - 0.6 \exp\left[-\frac{Re_D}{10^4}\right]. \tag{32}$$

It should be cautioned that (32) is valid for the ϵ-equation (17) only. When a different ϵ-equation is used to close (2) or a data set covering a larger Reynolds-number range

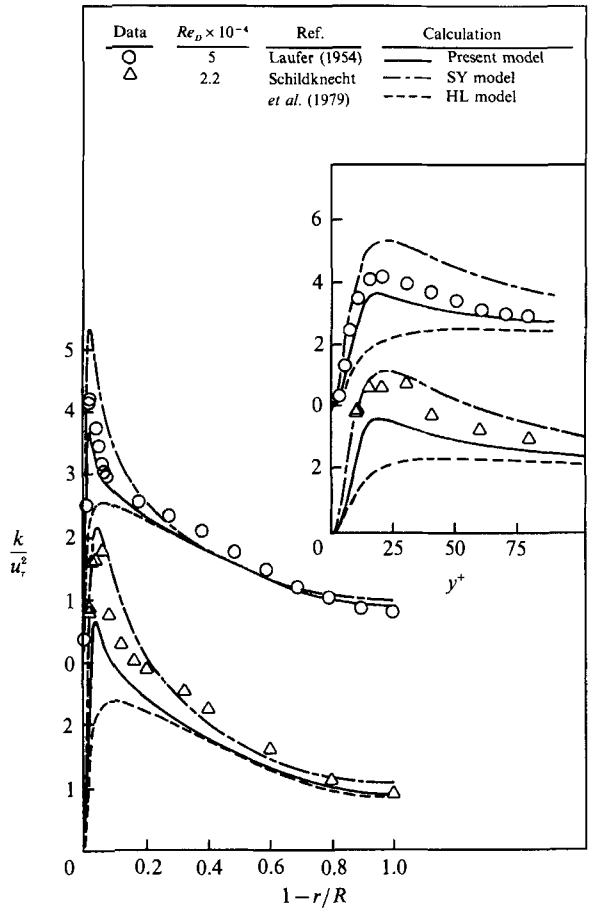

FIGURE 6. Comparison of Reynolds-stress closure calculations of k with data.

is used to calibrate σ, another σ expression might result. With the constant σ and α^* thus determined, the proposed near-wall Reynolds-stress and k–ϵ closures are validated against measurements and direct simulation data.

The comparison with Kim *et al.*'s (1987) data is shown in figures 1–3. The channel flow Reynolds number, Re, based on u_τ and $\frac{1}{2}H$ is 180, or $Re_D = U_0 H/\nu = 6600$. This gives a $\sigma \approx 0.7$ according to (32). Only the results of $-\overline{uv}$, the normal stresses and k are shown. These are plotted with $-\overline{uv}/u_\tau^2$, u'/u_τ, w'/u_τ, v'/u_τ and k/u_τ^2 versus $(1-y/H)$. Here, the prime is used to denote the r.m.s. value. The near-wall behaviour is shown in the inset of each figure in terms of y^+. Since the mean U only depends on $-\overline{uv}$ (see equation (24)), a correct $-\overline{uv}$ prediction also gives a correct prediction for U and vice versa. Therefore, it is not necessary to show the U comparison. As for ϵ, its comparison will be shown later in the k budget presentation, therefore, it is not necessary to repeat the ϵ comparison here.

In general, the overall comparisons are very good. The shapes of $-\overline{uv}$, w' and v' are essentially identical to those of direct simulation in the region $0 \leqslant y^+ < 10$ (figures 1 and 2). A small discrepancy exists in the comparison of u' and this leads to a corresponding slight disagreement in k (figure 3). Furthermore, the maximum u' is under-predicted while the maximum w' is over-predicted. The net result is an under-prediction of the maximum k. It should be pointed out that the maximum of

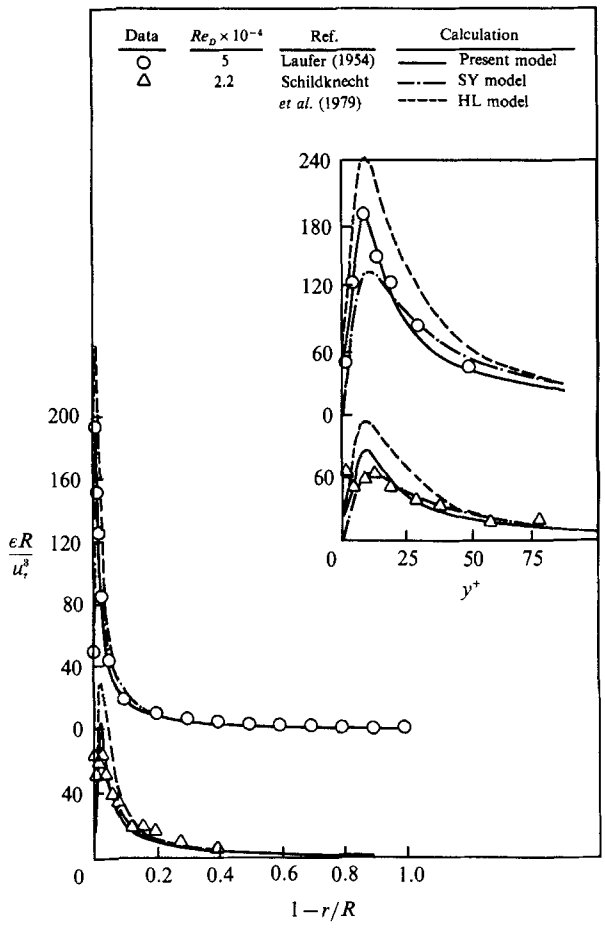

FIGURE 7. Comparison of Reynolds-stress closure calculations of ϵ with data.

k, u' and w' are influenced by α^*. This aspect of the proposed near-wall Reynolds-stress closure is consistent with other closures and could also be a consequence of the rather ad hoc ϵ-equation. More will be said about the ϵ-equation in the discussion of the comparison of the Reynolds-stress budgets.

Two sets of fully-developed pipe flow measurements at different Reynolds numbers are selected to further validate the present closures. These are the data of Laufer ($Re = 1052$ or $Re_D = 50000$) and Schildknecht *et al.* ($Re = 489$ or $Re_D = 21750$). At these Re_D, $\sigma \approx 1.0$ according to (32). The calculations are also compared with the Reynolds-stress predictions of Hanjalic & Launder (1976) and So & Yoo (1986), designated HL and SY, respectively, and the k–ϵ results of Chien (1982) and Lam & Bremhorst (1981), designated CH and LB, respectively.

The comparisons are made in terms of $U^+ = U/u_\tau$ versus $\ln y^+$, k/u_τ^2, u'/u_τ, v'/u_τ, w'/u_τ and $\epsilon R/u_\tau^3$ versus $(1-r/R)$ and the structure parameters $\overline{uv}/k$, $\overline{u^2}/k$, $\overline{v^2}/k$ and $\overline{w^2}/k$ versus $(1-r/R)$. Results for the Reynolds-stress closures are shown in figures 4–12 while predictions of the k–ϵ closures are compared in figures 13–17. The near-wall behaviour of all the parameters except U^+ are shown in the inset of each figure in terms of y^+ rather than $(1-r/R)$. Thus, the agreement, or lack thereof, between calculations and measurements in the near-wall region is clearly illustrated.

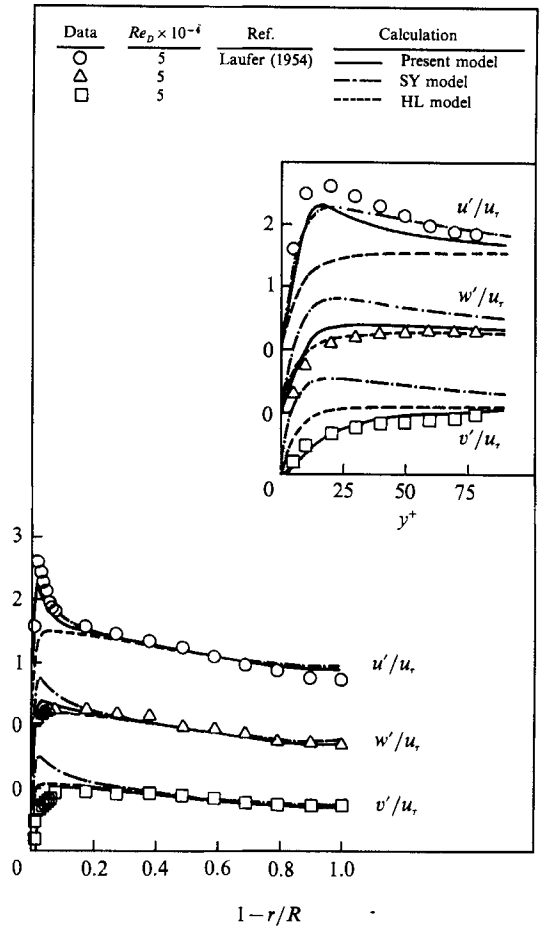

FIGURE 8. Comparison of Reynolds-stress closure calculations of the normal stresses with data.

As pointed out by So & Yoo (1986), the U^+ profiles obtained by integrating (24) using the measured $\overline{uv}$ are in much better agreement with the SY and CH closure results, thus indicating that there is a slight discrepancy between the measured $\overline{uv}$ and U in both sets of data. In view of this, the discrepancy shown in figure 4 between calculations and data cannot be attributed to model deficiency and all model calculations of U^+ can be considered to be in good agreement with measurements.

The linear behaviour of $-\overline{uv}$ is essentially guaranteed by (24). Therefore, all Reynolds-stress closure calculations are in excellent agreement with measurements in the region $(1-r/R) \geqslant 0.2$ (figure 5). The ability of the closures to mimic the near-wall behaviour of $-\overline{uv}$ is illustrated in the inset of figure 5. There again, the closures tested are doing very well, including the correct prediction of the Reynolds-number effect near a wall. On the other hand, the discrepancies between different closure calculations start to show up in the predictions of k and ϵ (figures 6 and 7). Among the three Reynolds-stress closures considered, the present calculations give the best agreement with data (figures 6 and 7). The SY closure over-predicts the maximum for both k and ϵ, while HL under-estimates both quantities. Both SY and HL closures give a slightly higher k than measurements in the pipe centre, compared to a correct prediction by the present closure (figure 6). This result confirms the

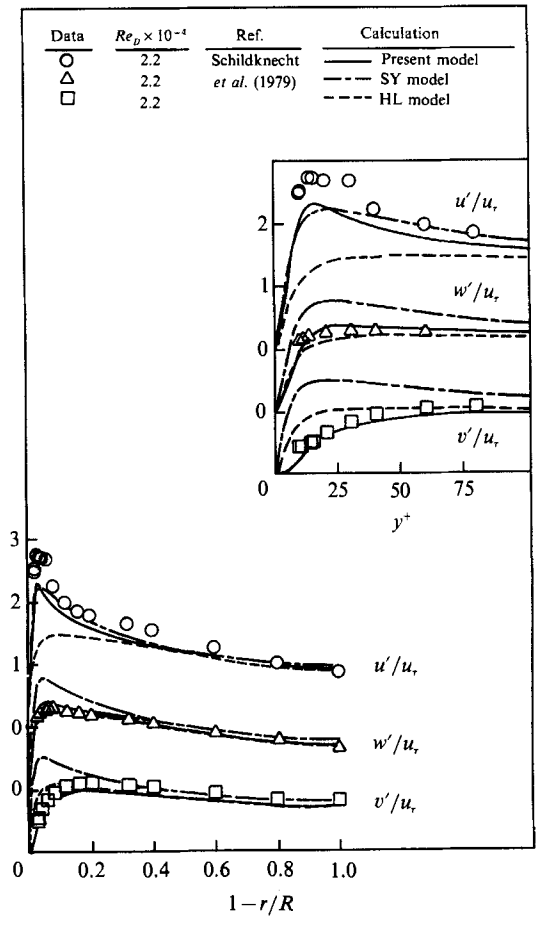

FIGURE 9. Comparison of Reynolds-stress closure calculations of the normal stresses with data.

necessity of modelling turbulent diffusion by an anisotropic model and the inclusion of the pressure diffusion effect in the modelled equations. The calculated anisotropic behaviour does not come from turbulent diffusion alone. It is also influenced by the modelling of Φ_{ij}. According to So & Yoo (1986), if Rotta's (1951) return-to-isotropy model is assumed for Φ_{ij} then k is also over-predicted in the pipe centre. This means that, even for such a simple shear flow, it is important to account for the mean-strain effect in the modelling of Φ_{ij}. It should be pointed out that the ϵ values at the wall obtained from Reynolds-stress closures depend on the boundary conditions imposed on ϵ. The SY closure uses Chien's ϵ-equation, therefore, the predicted ϵ goes to zero at the wall.

The calculated normal stresses for the two sets of data are shown in figures 8 and 9. It is in this comparison that the strength of the present Reynolds-stress closure really shows up. The model correctly predicts the anisotropic behaviour of the normal stresses in all three components and throughout the whole pipe. It also predicts the correct maximum for all the normal stresses including the effects of Reynolds number. All other closures fail to replicate the data correctly and essentially verify the importance of having an asymptotically correct model for Φ_{ij}^*. It should be pointed out that the correct near-wall ($y^+ < 10$) anisotropic behaviour

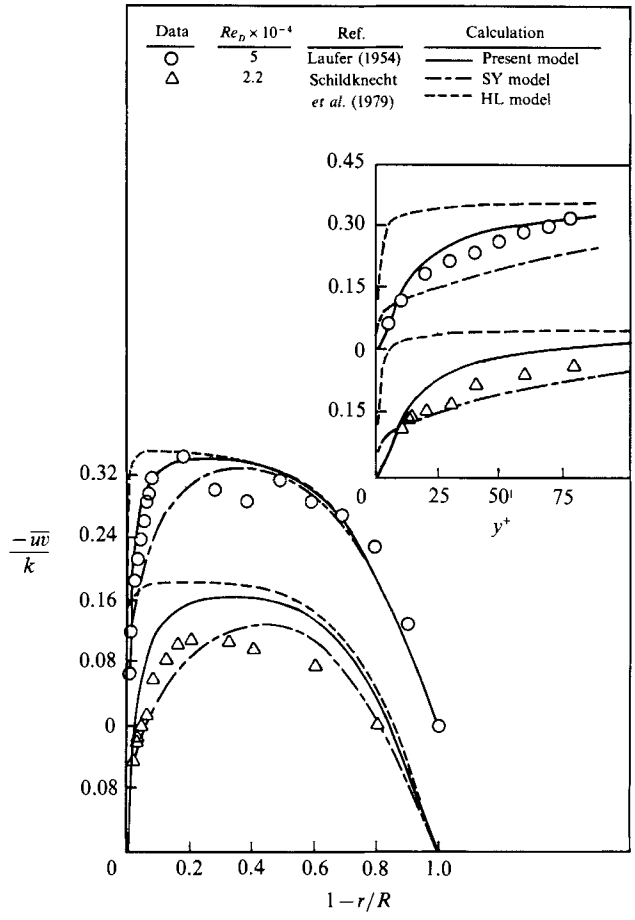

FIGURE 10. Comparison of Reynolds-stress closure calculations of $-\overline{uv}/k$ with data.

of u', v' and w' is affected by the first two terms in the model for $\Phi_{ij,w}$, while the correct maximum is influenced by the α^* term in the $\Phi_{ij,w}$ model. This is why the partitioning of Φ_{ij}^* into Φ_{ij}^D and Φ_{ij} is not valid for near-wall flow and Φ_{ij}^* has to be modelled as suggested in (14).

Further validation of the need to model Φ_{ij}^* in the near-wall region is provided by a comparison of the structure parameters (figures 10–12). The results show that the present Reynolds-stress closure not only provides the best predictions for all the structure parameters, but also reproduce the correct asymptotic behaviour of $\overline{u^2}/k$, $\overline{v^2}/k$ and $\overline{w^2}/k$ near the wall (figures 11 and 12). Both the HL and SY closures give a completely incorrect trend for the predictions of $\overline{u^2}/k$ and $\overline{v^2}/k$ in the region, $0 \leqslant y^+ \leqslant 25$. Furthermore, the present closure replicates the $\overline{v^2}/k$ behaviour in the $0 \leqslant y^+ \leqslant 75$ region correctly, which no other closure can do. This success is entirely due to the correct asymptotic behaviour of the $\Phi_{ij,w}$ and ϵ_{ij} models. Since Shima's (1988) proposed $\Phi_{ij,w}$ model does not have the proper asymptotic behaviour near a wall, it is expected that his model also cannot correctly predict the behaviour of $\overline{u^2}/k$, $\overline{v^2}/k$ and $\overline{w^2}/k$ in the near-wall region.

It should be pointed out that, in spite of numerous attempts, a convergent solution to the LB closure cannot be obtained. The difficulty is traced to an imbalance in the ϵ-equation in the near-wall region. Improving the initial guess, such as specifying the

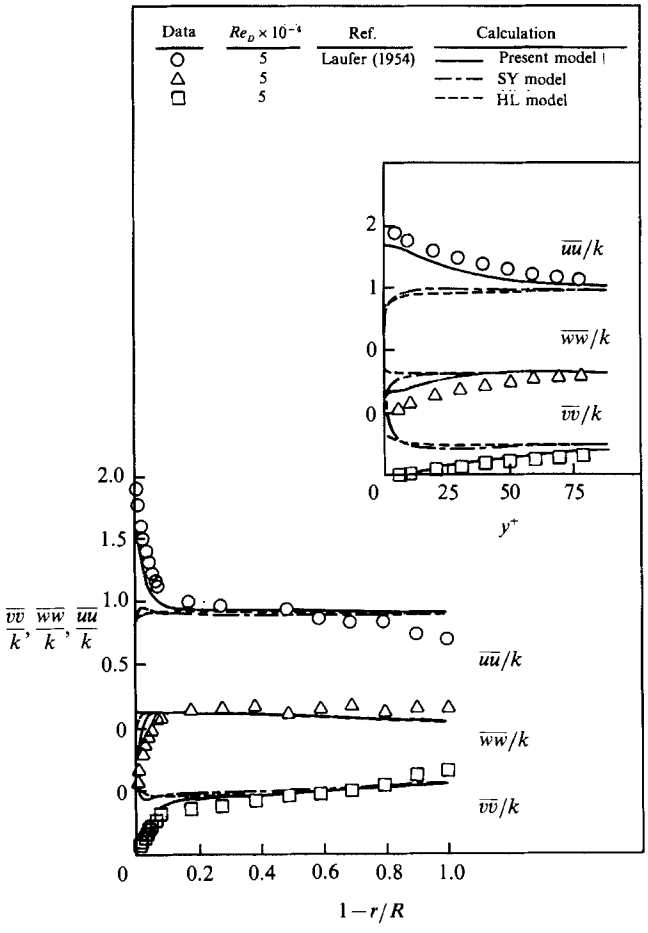

FIGURE 11. Comparison of calculated structure parameters with Laufer's data.

convergent solution of the CH closure as initial values for all variables, also fails to produce a convergent solution of the LB closure. This kind of difficulty does not exist for other k–ϵ closures that have been examined in this study. Therefore, subsequent comparisoins shown in figures 13–17 are only carried out between the present k–ϵ closure, the CH closure and measurements.

The mean velocity and shear stress predictions are compared in figures 13 and 14. As expected, both the present k–ϵ and CH closure calculations are in good agreement with measurements and the Reynolds-number effect is correctly predicted. The discrepancy noted in the mean U comparison (figure 13) is again traced to the slight inconsistency found between the measured $\overline{uv}$ and U in both sets of pipe flow data. There is also not much difference between the CH and the present k–ϵ closure in the prediction of k and ϵ (figures 15 and 16). Both closures cannot correctly predict the centreline k value and overestimate the maximum k (figure 15). Even though the k–ϵ equations for the present closure are asymptotically correct and those for the CH closure are not (because in the CH closure $\tilde{\epsilon}$ is required to behave like y^2 near a wall), the CH model predictions show better agreement with both sets of data. The reason lies in the choice of f_μ. In the CH closure, ν_t is actually given by $\nu_t = C_\mu f_\mu k^2/\tilde{\epsilon}$. Therefore, the present k–ϵ closure should use a slightly larger value for C_3 to compensate for the larger ϵ used in the definition of ν_t. The k result for the Laufer

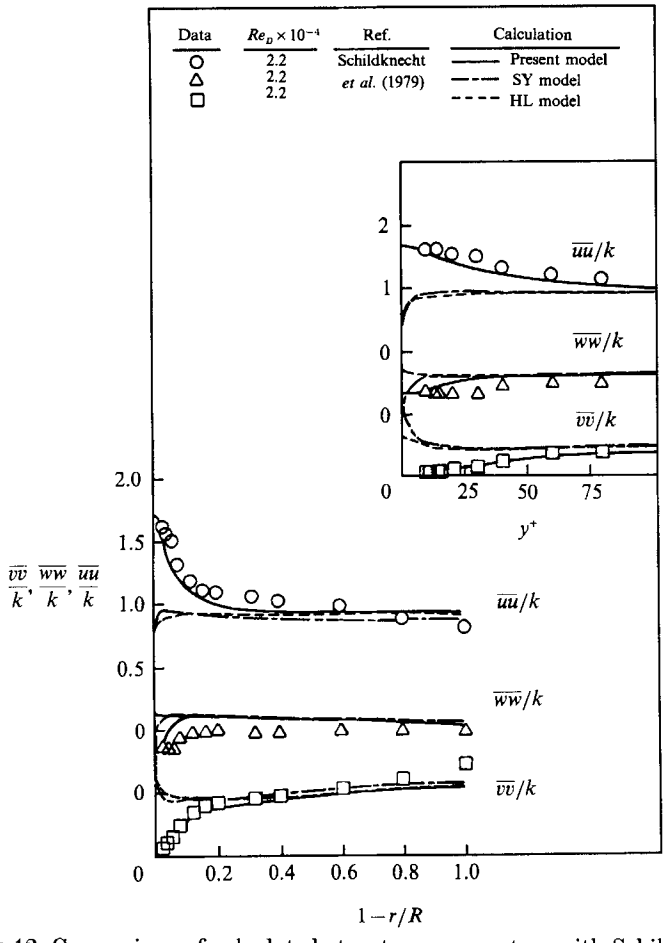

FIGURE 12. Comparison of calculated structure parameters with Schildknecht *et al.*'s data.

experiment obtained with $C_3 = 0.02$ is also shown in figure 15 and a much improved agreement with data is obtained. This shows that the incorrect near-wall behaviour of the CH closure is partially compensated by the choice of f_μ and the incorrect definition for ν_t. For the present k–ϵ closure, a much larger C_3 is called for. However, an optimization study has not been carried out to determine the correct value for C_3.

Finally, the k–ϵ closures gives a poor prediction of the structure parameter, $-\overline{uv}/k$ (figure 17). However, their predictions are better than the HL result (compare figures 10 and 17). Since the k–ϵ closures cannot replicate turbulent diffusion in all three directions correctly, there is no reason to expect them to give a correct prediction of $-\overline{uv}/k$. The poor performance of HL, on the other hand, is traced not to a lack of anisotropic turbulent diffusion but to an incorrect near-wall behaviour of the modelled equations.

8. Comparison of the Reynolds-stress budgets

Direct simulation of a fully-developed turbulent channel flow has recently been completed by Kim *et al.* (1987) and Mansour *et al.* (1988) at $Re = 180$. The results presented in the direct simulation studies included turbulence statistics (Kim *et al.* 1987) and budgets of the Reynolds stresses and the dissipation-rate (Mansour *et al.*

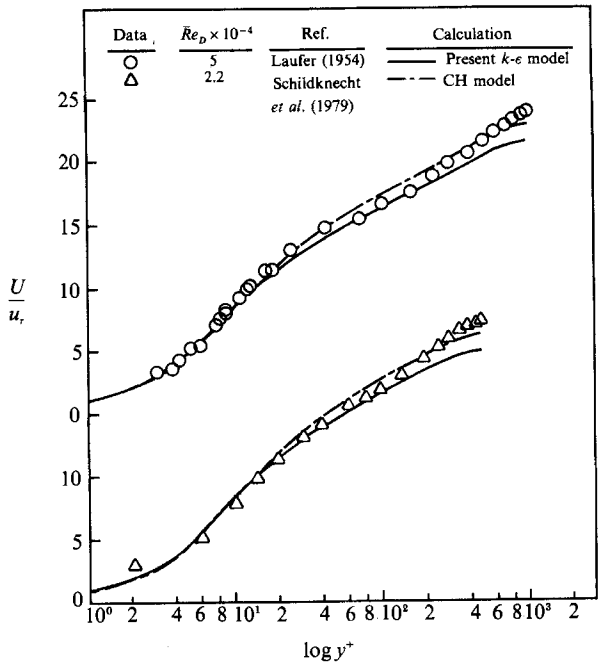

FIGURE 13. Comparison of k–ϵ closure calculations of U with data.

1988). The near-wall Reynolds-stress closure has already been validated for its ability to replicate the turbulence statistics. Since Mansour *et al.* (1988) have examined various models for D_{ij}^T, Φ_{ij} and ϵ_{ij} and their ability to predict the near-wall Reynolds-stress budgets and have come to the conclusion that they represent poor choices for the near-wall flow, a comparison of the present closure results with the calculations of Mansour *et al.* (1988) will further allow the individual models for D_{ij}^T, Φ_{ij}^* and ϵ_{ij} to be directly evaluated for their ability to replicate the flow in the near-wall region.

The comparisons of the various terms in the budgets of $\overline{u_i u_j}$ are shown in figures 18–21. In these figures, the model calculations are obtained assuming σ to be given by (32). According to Mansour *et al.* (1988), all the models considered for D_{ij}^T, Φ_{ij} and ϵ_{ij} compared favourably with the simulation data for $y^+ \geqslant 100$. However, substantial disagreement occurs in the near-wall region, $0 < y^+ < 50$. Since the present closure modifications are proposed for near-wall flows only, it would be appropriate to compare the near-wall closure's performance with simulation data in the region $0 < y^+ < 100$.

The terms in the budgets for $\overline{u^2}$ and $\overline{w^2}$ are compared in figures 18 and 19. In order to avoid clutter, the simulation data are shown in part (*a*) of each figure, while the model calculations are given in part (*b*). The general trends of D_{ij}^T and Φ_{ij}^* in the region $0 < y^+ < 100$ are approximately replicated by the near-wall turbulence closure. This implies that the proposed models for D_{ij}^T and Φ_{ij}^* are quite appropriate. However, the behaviour of $-\epsilon_{ij}$, in particular that of $-\epsilon_{11}$ and $-\epsilon_{33}$, is not reproduced correctly. The major difference occurs in the region $0 \leqslant y^+ < 30$. Direct simulation results show that the maximum of $-\epsilon_{11}$ and $-\epsilon_{33}$ occurs at the wall, while the closure results indicate the maximum of $-\epsilon_{11}$ and $-\epsilon_{33}$ at $y^+ \approx 10$. Furthermore, the calculated wall values of $-\epsilon_{11}$ and $-\epsilon_{33}$ vary from $\frac{1}{3}$ to $\frac{1}{2}$ of the simulation data. In spite of this, the balance between $-\epsilon_{ii}$ and D_{ii}^v at the wall is satisfied. Consequently, the closure results

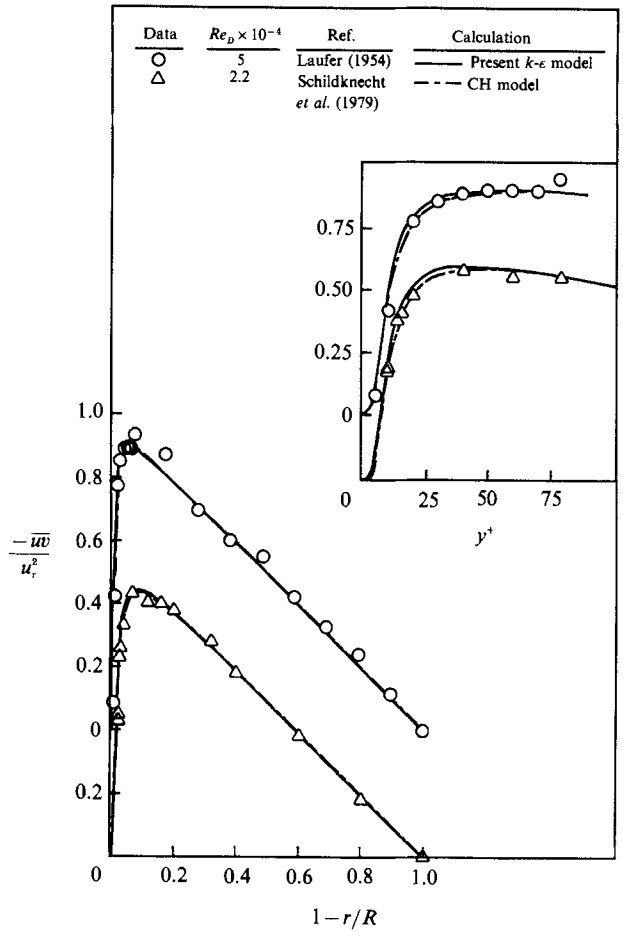

FIGURE 14. Comparison of k–ϵ closure calculations of $\overline{uv}$ with data.

for D_{11}^{ν} and D_{33}^{ν} at the wall are substantially smaller than those obtained from simulation. The behaviour of the various closure calculated terms in the budgets of $\overline{u_i u_j}$, in general, are in qualitative agreement with direct simulation data. There are two exceptions, though. These are the magnitudes of Φ_{22}^{*} and $-\epsilon_{22}$ which are about two to three times larger than the simulation data in the region $y^+ < 100$. This is due to the fact that the high-Reynolds-number model for ϵ_{ij} is isotropic, while the direct simulation results for $-\epsilon_{11}$, $-\epsilon_{22}$, $-\epsilon_{33}$ show that they are quite anisotropic. The anisotropy extends over the whole channel. However, these discrepancies do not seem to affect the overall prediction of the turbulence statistics (figures 15 and 16).

The comparisons of the terms in the budgets of k and $\overline{uv}$ are shown in figures 20 and 21. In figure 20, $D_k^{\nu} = \frac{1}{2}D_{ii}^{\nu}$, $D_k^{T} = \frac{1}{2}D_{ii}^{T}$, $P_k = \frac{1}{2}P_{ii}$, $\Phi_k^{*} = \frac{1}{2}\Phi_{ii}^{*}$ and $\epsilon = \frac{1}{2}\epsilon_{ii}$. As expected, a discrepancy in the k budget comparison also occurs in the behaviour of $-\epsilon$ near and at the wall. The calculated wall value of $-\epsilon$ is about 40% of the simulation data. As a result, the behaviour of Φ_k^{*} in the region $y^+ < 20$ is incorrect; slightly negative away from the wall as compared to slightly positive in the simulation result. The near-wall trend of D_k^{T}, though not the magnitude, is correctly reproduced by the model and shows that a gradient-diffusion assumption can be used to model D_k^{T}. The magnitude of D_k^{T}, of course, is affected by the value of C_s, which for the present case is chosen as 0.11. A greater value of C_s would increase the

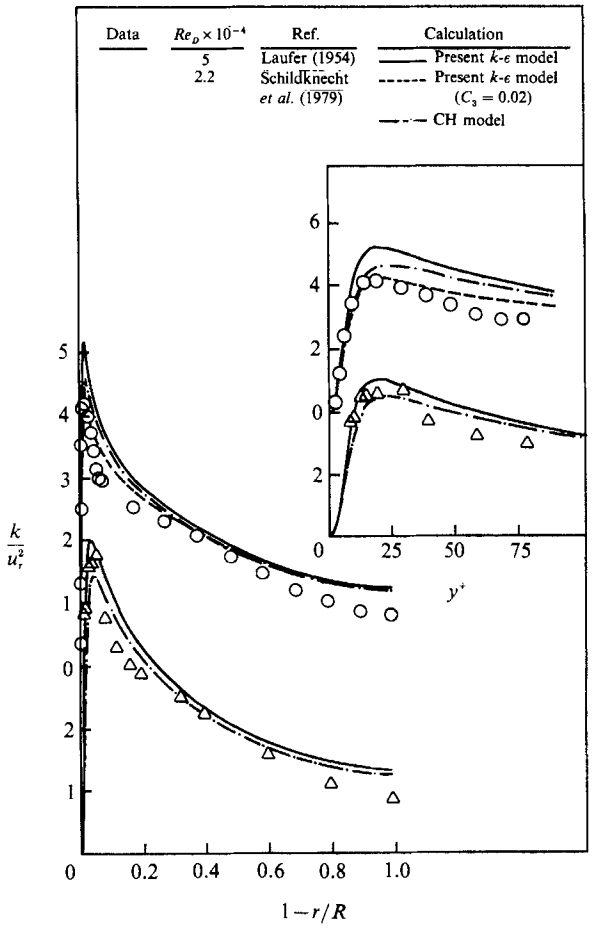

FIGURE 15. Comparison of k–ϵ closure calculations of k with data.

magnitude of D_k^T, thus improving the agreement between model calculation and direct simulation. The comparison of the terms in the budget of $\overline{uv}$ (figure 21) is slightly more favourable than those shown in figures 18–20. In particular, the model calculation of the behaviour of Φ_{12}^* agrees with the direct simulation result, even the maximum reached by Φ_{12}^* is in agreement. This means that the proposed near-wall Φ_{ij}^* model is reasonable, at least for the channel flow considered, and further substantiates the need to model Φ_{ij}^* rather than Φ_{ij}. The split of Φ_{ij}^* into Φ_{ij} and Φ_{ij}^p and the neglect of Φ_{ij}^p may be appropriate for flows far away from a wall, however, it is not valid for near-wall flows. This conclusion is substantiated by the findings of Mansour *et al.* (1988) and the present study. The calculated trend of D_{12}^T is similar to the simulation data but its maximum is about three times smaller than the simulation result. In view of these findings, it can be concluded that the correct modelling of ϵ_{ij} is crucial to the prediction of the terms in the budgets of $\overline{u_i u_j}$. Since the model for ϵ_{ij} invariably involves ϵ, the modelled equation for ϵ becomes an important element in any Reynolds-stress closure.

In order to further examine the effects of the modelled ϵ-equation on the $\overline{u_i u_j}$ budgets, $\sigma = 0$ is assumed and the calculation is repeated. The terms in the budget of $\overline{u^2}$ are shown in figure 18(*c*), while those of k are shown in figure 20(*c*). It can be seen that neglecting the extra ϵ generation due to ψ results in a $-\epsilon_{11}$ behaviour very

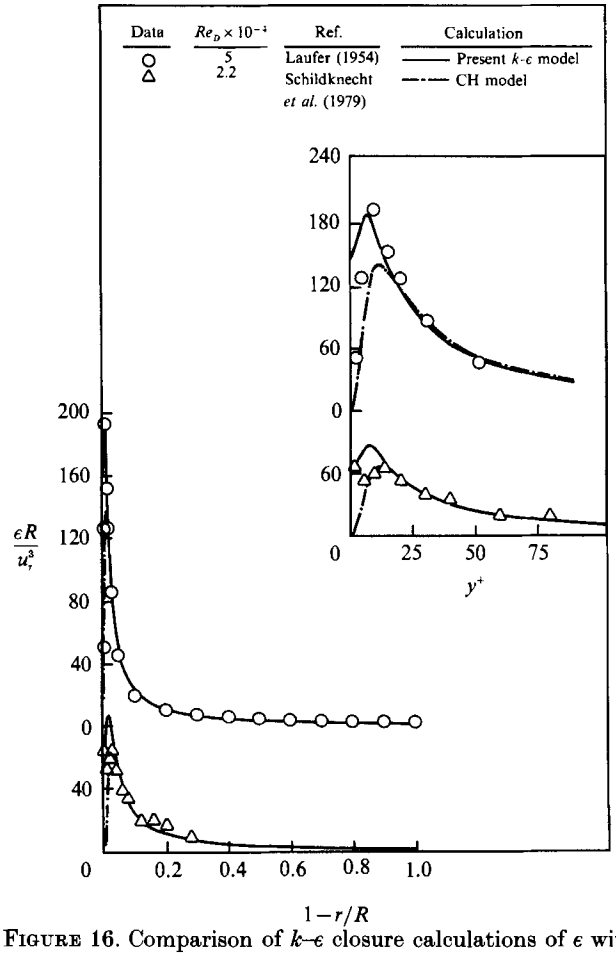

FIGURE 16. Comparison of k–ϵ closure calculations of ϵ with data.

similar to that obtained from direct simulation. The maximum of $-\epsilon_{11}$ now appears at the wall and its value is equal to that given by direct simulation. Furthermore, D_{11}^{ν} at the wall also increases to match the wall value of $-\epsilon_{11}$. The magnitude and behaviour of Φ_{11}^{*} are not affected by this change in σ value. On the other hand, the prediction of D_{11}^{T} has been improved by setting $\sigma = 0$ and the result becomes similar to that of direct simulation. Since $-\epsilon_{33}$ is small compared to $-\epsilon_{11}$, the behaviour of ϵ is dominated by the behaviour of $-\epsilon_{11}$. Consequently, in the comparison of the terms in the budget of k, the behaviour of the $-\epsilon$ term for the $\sigma = 0$ case is also in agreement with the direct simulation data (compare figures 20*a* and 20*c*). Even though σ has a significant effect on the budgets of $\overline{u^2}$ and k, its influence on the budgets of $-\overline{uv}$ and $\overline{w^2}$ is small. The results are essentially the same as those shown in figures 10(*b*) and 21(*b*). In spite of the improvements noted in the Reynolds-stress budgets, setting $\sigma = 0$ gives predicted turbulence statistics that are in poor agreement with those shown in figures 1–3, especially in the region $0 \leqslant y^+ < 20$. This suggests that the weakest link in the present near-wall Reynolds-stress closure is the ϵ-equation. Therefore, further improvements in turbulence modelling should be directed at modifying this equation rather than at the $\overline{u_i u_j}$ equations. On the other hand, if the objective is to predict the turbulence statistics alone, then the present ϵ-equation is quite adequate.

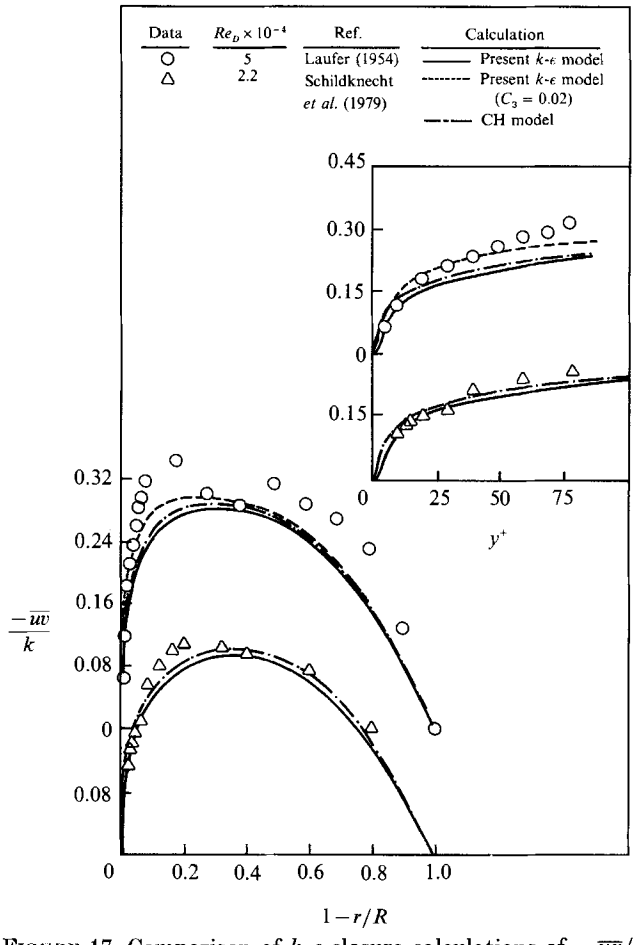

FIGURE 17. Comparison of k–ϵ closure calculations of $-\overline{uv}/k$ with data.

9. Discussion

The present study proposes an approach for the derivation of a near-wall Reynolds-stress closure. It is based on the premise that the modelled equations should have the same near-wall behaviour as the original $\overline{u_i u_j}$ equations. A further stipulation is that the models for the individual terms in the $\overline{u_i u_j}$ equations should be Reynolds-number independent far away from a wall. Therefore, once the high-Reynolds-number models are specified for the $\overline{u_i u_j}$ equations, the near-wall corrections of these models can be deduced to satisfy the resultant near-wall behaviour of each term in the $\overline{u_i u_j}$ equations. The near-wall Reynolds-stress closure thus derived is dependent on the high-Reynolds-number models used. If physically more accurate high-Reynolds-number models for D_{ij}^T, Φ_{ij}^* and ϵ_{ij} are available, such as models deduced from stress invariants, the present approach can again be used to derive the required near-wall modifications to these models. For example, if the model suggested by Lumley (1980) for Φ_{ij}^* is used instead of Launder *et al.*'s model, the present approach can be applied to deduce a near-wall correction for Lumley's model. In that sense, models that satisfied the realizability condition are equally suitable for the present approach. The Launder *et al.* model is chosen here, because of its simplicity, general acceptance and wide applicability, to illustrate the methodology of deducing a near-wall closure.

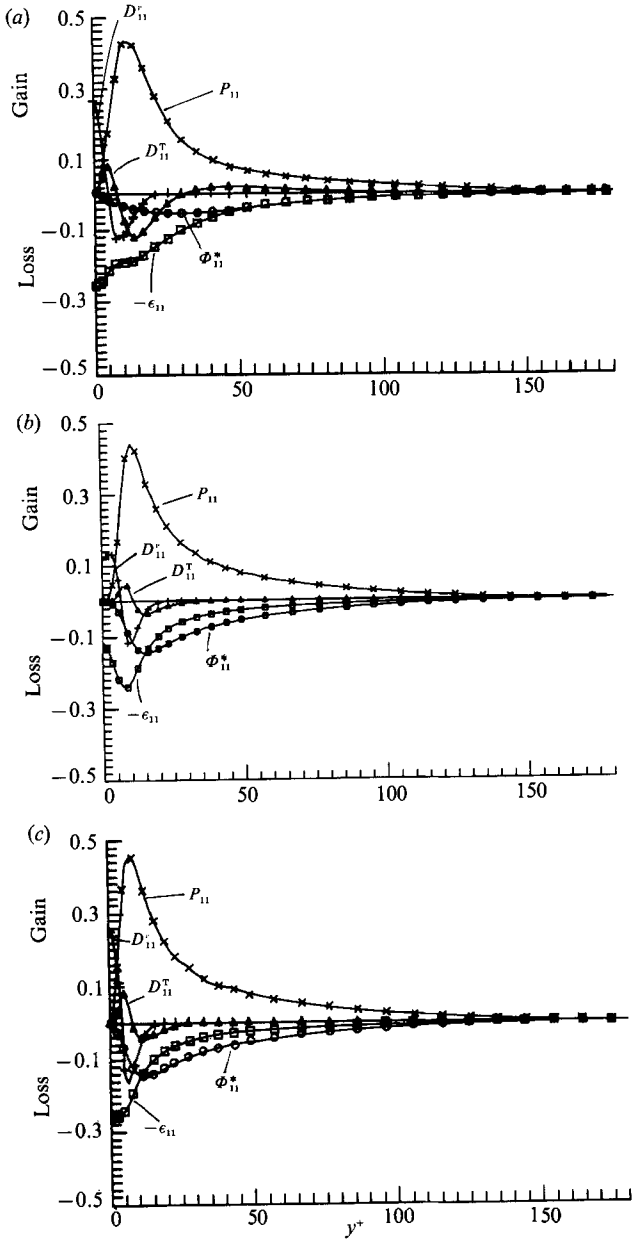

FIGURE 18. Comparison of the terms in the budget of $\overline{u^2}$; (*a*) direct simulation, (*b*) turbulence model, σ given by equation (32), (*c*) turbulence model, $\sigma = 0$.

Up to now, only two-dimensional data has been used to validate the proposed near-wall Reynolds-stress closure. Therefore, its suitability for three-dimensional flows is still in question. However, indirect evidence of its suitability for three-dimensional flows can be found in other studies. A first attempt to use near-wall Reynolds-stress closure to calculate three-dimensional flows was made by Yoo *et al.* (1991). They applied the closure of So & Yoo (1986) to predict the developing entrance flow in an axially rotating pipe. Good agreement with measurements is obtained for the mean velocities as well as for the Reynolds stresses for several

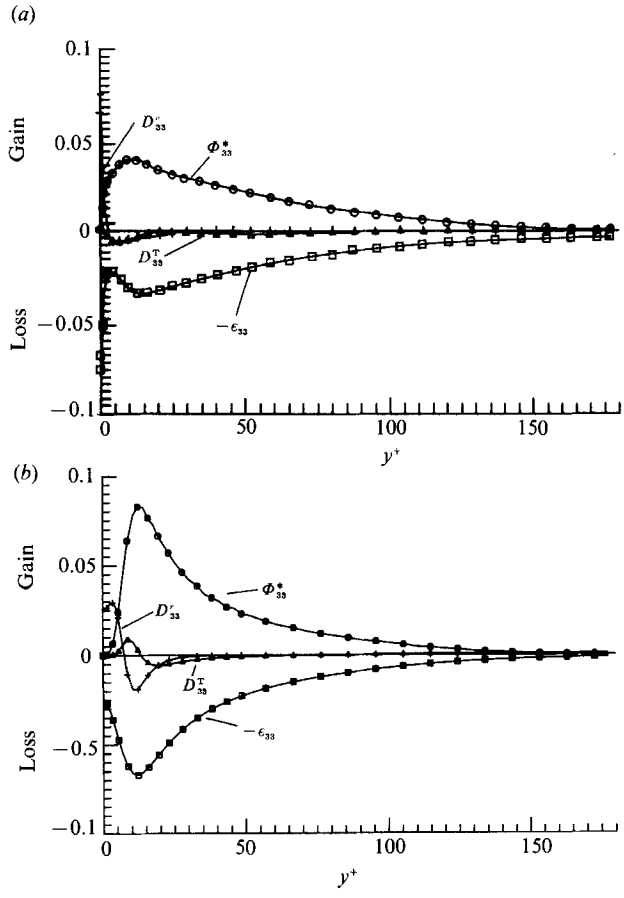

FIGURE 19. Comparison of the terms in the budget of $\overline{w^2}$; (*a*) direct simulation, (*b*) turbulence model, σ given by equation (32).

different pipe rotation rates. The present model has also been applied by Lai *et al.* (1990) to calculate three-dimensional flows in a curved pipe. A substantial improvement in the predictions of the turbulence statistics is noted compared to the results obtained assuming conventional wall functions and high-Reynolds-number models for D^T_{ij}, Φ_{ij} and ϵ_{ij}. Since the present closure performs better than the So & Yoo (1986) closure in the near-wall region, in particular, in the prediction of the normal stresses, it should be more suitable for three-dimensional flows than the closure of So & Yoo (1986). Nevertheless, direct verification of the closure beyond the study of Lai *et al.* (1990) is necessary before it can be claimed to be valid for three-dimensional flows.

Finally, the success of the near-wall Reynolds-stress closure depends, to a large extent, on the correctness of the ϵ-equation. Conflicting results concerning the suitability of the ψ term in the ϵ-equation are obtained in the present study. On the one hand, inclusion of $\psi(\sigma \neq 0)$ in the ϵ-equation gives rise to a correct prediction of the turbulence statistics, while the neglect of $\psi(\sigma = 0)$ leads to a correct replication of the behaviour of $-\epsilon_{11}$ and $-\epsilon$ in the budgets of $\overline{u^2}$ and k. Therefore, further work is needed to improve the rather ad hoc ϵ-equation so that both the turbulence statistics and the terms in the budgets of $\overline{u_i u_j}$ are in agreement with measurements as well as direct stimulation data. Nevertheless, extension of this

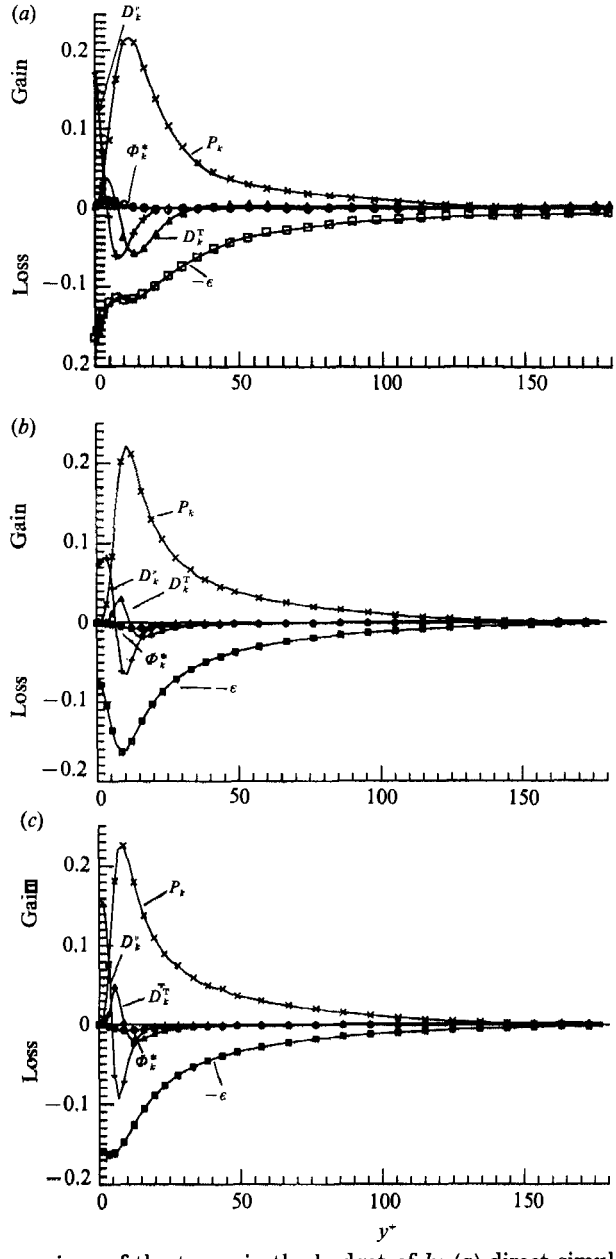

FIGURE 20. Comparison of the terms in the budget of k; (*a*) direct simulation, (*b*) turbulence model, σ given by equation (32), (*c*) turbulence model, $\sigma = 0$.

approach to model two-dimensional turbulent heat transfer near a wall indicates that the resultant near-wall heat flux model gives excellent prediction of the near-wall vertical heat flux (Lai & So 1990).

10. Conclusions

An asymptotically correct near-wall Reynolds-stress closure has been proposed. In order to achieve coincidence of all terms in the Reynolds-stress equations at the wall, it is found that the velocity-pressure-gradient correlation should not be partitioned

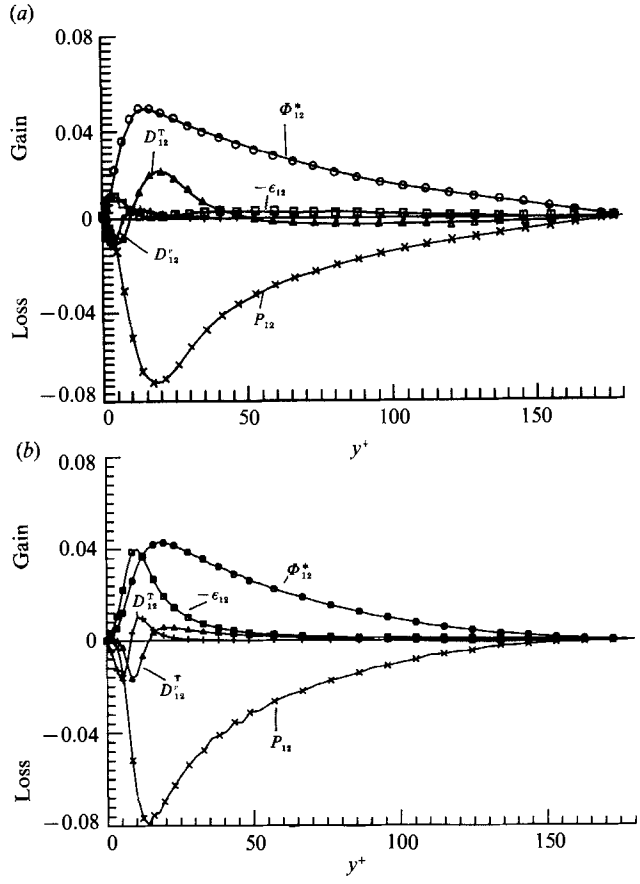

FIGURE 21. Comparison of the terms in the budget of $\overline{uv}$; (*a*) direct simulation, (*b*) turbulence model, σ given by equation (32).

into a pressure diffusion part, which is neglected, and a pressure redistribution part, which is modelled. The pressure diffusion part is important in the near-wall region and is responsible for the anisotropic turbulence behaviour near the wall. However, it is indeed negligible far away from the wall. This understanding is used to formulate a model for the velocity-pressure-gradient correlation that has a non-zero trace in the near-wall region but asymptotes correctly to the modelled pressure redistribution tensor far away from the wall. The viscous dissipation model is also modified to reproduce the correct near-wall behaviour. Thus formulated, the modelled and exact terms in the Reynolds-stress equations are in balance near a wall, just as they should be in the original equations. Closure of the Reynolds-stress equations is then provided by the modification of an existing ϵ-equation that is also asymptotically correct as the wall is approached. A by-product of this study is an asymptotically correct k–ϵ closure obtained by contracting the modelled Reynolds-stress equations and invoking the assumption of gradient transport.

In view of the rather ad hoc nature of the ϵ-equation, the model constants introduced by the near-wall closures are first investigated for Reynolds-number dependence. As indicated by Mansour *et al.* (1989), σ is found to depend on Re_D and a preliminary expression is proposed for σ. This is then used to calculate the channel flow data of Kim *et al.* (1987) and the pipe flow measurements of Laufer (1954) and

of Schildknecht *et al.* (1979) in a range of Re varying from 180 to 1052. The calculated turbulence statistics compare favourably with those obtained from direct simulation. As for the comparisons with pipe flow measurements, it is found that by virtue of the isotropic assumption inherent in the gradient transport approximation, the k–ϵ closure cannot correctly predict the turbulence energy at the pipe centre. Also, the damping function proposed for the eddy viscosity has a great effect on the predicted maximum turbulent kinetic energy near the pipe wall. On the other hand, the near-wall Reynolds-stress closure results substantiate the hypothesis that the velocity-pressure-gradient correlation should be modelled in its entirety in the near-wall region. Only then can the various terms in the modelled Reynolds-stress equations be balanced in the near-wall region just like the exact equations and the anisotropic behaviour of the normal stresses be predicted correctly near the wall. All other near-wall Reynolds-stress closures that rely on the modelling of the pressure redistribution part alone fail to correctly predict the near-wall behaviour of the normal stresses.

Further verification of the near-wall Reynolds-stress closure is carried out with the Reynolds-stress budgets of Mansour *et al.* (1988). In this validation, the importance of having a correct ϵ-equation in the closure is clearly brought out. For example, the presence or absence of extra ϵ generation in the ϵ-equation affects the predictions differently. If the extra ϵ generation is present, the mean flow and the turbulence statistics are predicted correctly. On the other hand, in the absence of ψ, the $-\epsilon$ and $-\epsilon_{11}$ behaviour in the budgets of k and $\overline{u^2}$ is replicated correctly compared to the simulation data. The behaviour of other terms in the budgets of $\overline{u_i u_j}$ is also affected by this extra ϵ generation term. This implies that a more physically based ϵ-equation is required. However, the turbulence statistics are not significantly affected by the ϵ-equation as long as σ is taken to be Reynolds-number dependent as suggested by Mansour *et al.* (1989).

This work was partially supported by the Naval Weapons Center, China Lake, California under Contract No. N60530-85-C-0191, by the Naval Ship Research and Development Center, Annapolis, Maryland under Contract No. N00167-86-K-0075 and by NASA Langley Research Centre under Grant No. NAG-1-1080.

REFERENCES

Amano, R. S. & Goel, P. 1987 Investigation of third-order closure model of turbulence for the computation of incompressible flows in a channel with a backward-facing step. *Trans. ASME* I: *J. Fluids Engng* **109**, 424–428.

Chien, K. Y. 1982 Predictions of channel and boundary layer flows with a low-Reynolds-number two-equation model of turbulence. *AIAA J.* **20**, 33–38.

Cormack, D. E., Leal, L. G. & Steinfeld, J. H. 1978 An evaluation of mean Reynolds stress turbulence models: the triple velocity correlation. *Trans. ASME* I: *J. Fluids Engng* **100**, 47–54.

Daly, B. J. & Harlow, F. H. 1970 Transport equations in turbulence. *Phys. Fluids* **13**, 2634–2649.

Driest, E. R. van 1956 On turbulent flow near a wall. *J. Aero. Sci.* **23**, 1007–1011.

Hanjalic, K. & Launder, B. E. 1972 A Reynolds-stress model of turbulence and its application to thin shear flows. *J. Fluid Mech.* **52**, 609–638.

Hanjalic, K. & Launder, B. E. 1976 Contribution towards a Reynolds-stress closure for low-Reynolds-number turbulence. *J. Fluid Mech.* **74**, 593–610.

Hoffmann, G. H. 1975 Improved form of the low-Reynolds number k–ϵ turbulence model. *Phys. Fluids* **18**, 309–312.

Jones, W. P. & Launder, B. E. 1972 The prediction of laminarization with a two-equation model of turbulence. *Intl J. Heat Mass Transfer* **15**, 301–314.

KEBEDE, W., LAUNDER, B. E. & YOUNIS, B. A. 1985 Large amplitude periodic pipe flow: a second-moment closure study. *Proc. 5th Symp. Turbulent Shear Flows, Ithaca, NY*, pp. 16.23–16.29.

KIM, J., MOIN, P. & MOSER, R. 1987 Turbulence statistics in fully developed channel flow at low Reynolds number. *J. Fluid Mech.* **177**, 133–186.

KOLMOGOROV, A. N. 1941 Local structure of turbulence in incompressible viscous fluid for very large Reynolds number. *Dokl. Akad. Nauk SSSR* **30**, 299–303.

KREPLIN, H. P. & ECKELMANN, H. 1979 Behavior of the three fluctuating velocity components in the wall region of a turbulent channel flow. *Phys. Fluids* **22**, 1233–1239.

LAI, Y. G. & SO, R. M. C. 1990 Near-wall modelling of turbulent heat fluxes. *Intl J. Heat Mass Transfer* **33**, 1429–1440.

LAI, Y. G., SO, R. M. C., ANWER, M. & HWANG, B. C. 1990 Modelling of turbulent curved-pipe flows. Presented at the *Intl Symp. on Engineering Turbulence Modelling and Measurements, Dubrovnik, Yugoslavia, September* 24–28.

LAI, Y. G., SO, R. M. C. & HWANG, B. C. 1989 Calculation of planar and conical diffuser flows. *AIAA J.* **27**, 542–548.

LAM, C. K. G. & BREMHORST, K. A. 1981 Modified form of the k–ϵ model for predicting wall turbulence. *Trans. ASME* I: *J. Fluids Engng* **103**, 456–460.

LAUFER, J. 1954 The structure of turbulence in fully developed pipe flow. *NACA Rep.* 1174.

LAUNDER, B. E. 1986 Low-Reynolds number turbulence near walls. *UMIST, Mech. Engng Dept Rep.* TFD/86/4.

LAUNDER, B. E., REECE, G. J. & RODI, W. 1975 Progress in the development of a Reynolds-stress turbulence closure. *J. Fluid Mech.* **68**, 537–566.

LAUNDER, B. E. & REYNOLDS, W. C. 1983 Asymptotic near-wall stress dissipation rates in a turbulent flow. *Phys. Fluids* **26**, 1157–1158.

LAUNDER, B. E. & TSELEPIDAKIS, D. P. 1988 Contribution to the second-moment modelling of sublayer turbulent transport. *Zaric Memorial Intl Seminar on Near-Wall Turbulence, Dubrovnik, Yugoslavia, May* 16–20.

LUMLEY, J. L. 1980 Second order modelling of turbulent flow. *Prediction Methods for Turbulent Flows* (ed. W. Kollmann), pp. 1–31. Hemisphere.

MANSOUR, N. N., KIM, J. & MOIN, P. 1988 Reynolds-stress and dissipation-rate budgets in a turbulent channel flow. *J. Fluid Mech.* **192**, 15–44.

MANSOUR, N. N., KIM, J. & MOIN, P. 1989 Near-wall k–ϵ turbulence modelling. *AIAA J.* **27**, 1068–1073.

NA, T. Y. 1979 *Computation Methods in Engineering Boundary Value Problems.* Academic.

NIKJOOY, M. & SO, R. M. C. 1989 On the modelling of scalar and mass transport in combustor flows. *Intl J. Numer. Meth. Engng* **28**, 861–877.

PATEL, V. C., RODI, W. & SCHEUERER, G. 1985 Turbulence models for near-wall and low-Reynolds-number flows: a review. *AIAA J.* **23**, 1308–1319.

PRUD'HOMME, M. & ELGHOBASHI, S. 1983 Prediction of wall-bounded turbulent flows with an improved version of a Reynolds-stress model. *Proc. 4th Symp. Turbulent Shear Flows, Karlsruhe, FRG*, pp. 1.7–1.12.

REYNOLDS, W. C. 1976 Computation of turbulent flows. *Ann. Rev. Fluid Mech.* **8**, 183–208.

ROTTA, J. C. 1951 Statistiche Theorie Nichthomogener Turbulenz. *Z. Phys.* **129**, 547–572; also **131**, 51–77.

SCHILDKNECHT, M., MILLER, J. A. & MEIER, G. E. A. 1979 The influence of suction on the structure of turbulence in fully-developed pipe flow. *J. Fluid Mech.* **90**, 67–107.

SHIMA, N. 1988 A Reynolds-stress model for near-wall and low-Reynolds-number regions. *J. Fluids Engng* **110**, 38–44.

SHIR, C. C. 1973 A preliminary numerical study of atmospheric turbulent flows in the idealized planetary boundary layer. *J. Atmos. Sci.* **30**, 1327–1339.

SO, R. M. C., LAI, Y. G., HWANG, B. C. & YOO, G. J. 1988 Low-Reynolds-number modelling of flows over a backward-facing step. *Z. angew. Math. Phys.* **39**, 13–27.

So, R. M. C. & Yoo, G. J. 1986 On the modelling of low-Reynolds-number turbulence. *NASA* CR-3994.

So, R. M. C. & Yoo, G. J. 1987 Low-Reynolds-number modelling of turbulent flows with and without wall transpiration. *AIAA J.* **25**, 1556–1564.

Yoo, G. J. & So, R. M. C. 1989 Variable density effects on axisymmetric sudden-expansion flows. *Intl J. Heat Mass Transfer* **32**, 105–120.

Yoo, G. J., So, R. M. C. & Hwang, B. C. 1991 Calculation of developing turbulent flows in a rotating pipe. *J. Turbomachinery*, to appear.